axioms

MDPI

Article

Fractional Solitons for Controlling Wave Dynamics in Fluids and Plasmas

Muhammad Tehseen [1], Emad K. Jaradat [2], Elsayed M. Abo-Dahab [3] and Hamood Ur Rehman [4,*]

[1] Department of Mathematics, University of Okara, Okara 56300, Pakistan; tehseen.saleem115@gmail.com
[2] Department of Physics, Faculty of Science, Imam Mohammad Ibn Saud Islamic University (IMSIU), Riyadh 11623, Saudi Arabia; ekyjaradat@imamu.edu.sa
[3] Mathematics Department, Faculty of Science, South Valley University, Qena 83523, Egypt; elsayed.khodeari@sci.svu.edu.eg
[4] Center for Theoretical Physics, Khazar University, 41 Mehseti Street, Baku AZ1096, Azerbaijan
* Correspondence: hamood84@gmail.com

Abstract

This paper presents soliton solutions of the fractional (2+1)-dimensional Davey–Stewartson equation based on a local fractional derivative to represent wave packet propagation in dispersive media under both spatial and temporal effects. The importance of this work is in demonstrating how fractional derivatives represent a more capable modeling tool compared to conventional integer-order methods since they include anomalous dispersion, nonlocal interactions, and memory effects typical in most physical systems in nature. The main objective of this research is to build and examine a broad family of soliton solutions such as bright, dark, singular, bright–dark, and periodic forms, and to explore the influence of fractional orders on their amplitude, width, and dynamical stability. Specific focus is given to the comparison of the behavior of fractional-order solutions with that of traditional integer-order models so as to further the knowledge on fractional calculus and its role in governing nonlinear wave dynamics in fluids, plasmas, and other multifunctional media. Methodologically, this study uses the fractional complex transform together with a new mapping technique, which transforms the fractional Davey–Stewartson equation into solvable nonlinear ordinary differential equations. Such a systematic methodology allows one to derive various families of solitons and form a basis for investigation of nonlinear fractional systems in the general case. Numerical simulations, given in the form of three-dimensional contour maps, density plots, and two-dimensional, demonstrate stability and propagation behavior of the derived solitons. The findings not only affirm the validity of the devised analytic method but also promise possibilities of useful applications in fluid dynamics, plasma physics, and nonlinear optics, where wave structure manipulation using fractional parameters can result in increased performance and novel capabilities.

Keywords: fractional (2+1)-dimensional Davey–Stewartson equation (DSE); new mapping method (NMM); local fractional derivative; soliton solutions

MSC: 35C07; 35C08; 35G20; 35Q53

check for updates

Academic Editor: Feliz Manuel Minhós

Received: 31 August 2025
Revised: 21 September 2025
Accepted: 25 September 2025
Published: 20 October 2025

Citation: Tehseen, M.; Jaradat, E.K.; Abo-Dahab, E.M.; Rehman, H.U. Fractional Solitons for Controlling Wave Dynamics in Fluids and Plasmas. *Axioms* **2025**, *14*, 772. https://doi.org/10.3390/axioms14100772

Copyright: © 2025 by the authors. Licensee MDPI, Basel, Switzerland. This article is an open access article distributed under the terms and conditions of the Creative Commons Attribution (CC BY) license (https://creativecommons.org/licenses/by/4.0/).

1. Introduction

In recent years, remarkable advancements have been made in the theory of solitons, highlighting their importance in the study of nonlinear systems. This work is devoted to exploring optical solitons and further exact solutions in magneto-optic wave-guides,

which are displayed through a coupled system of nonlinear generalized Schrödinger (NLS) equations including two different forms of nonlinearity. Optical solitons serve as a cornerstone in the field of telecommunications and play a vital role in nonlinear optics due to their inherent stability and robustness. Soliton models are extensively utilized in a wide range of applications including solitary wave-based communication systems, optical pulse compressors, fiber-optic amplifiers, and many other photonic devices. Fundamentally, solitons arise from the delicate balance between nonlinearity tending to steepen the wave profile and dispersion which tends to spread the wave. The derivation of exact traveling wave solutions for nonlinear partial differential equations (PDEs) is necessary in understanding and analyzing nonlinear physical phenomena. Among these, the nonlinear Schrödinger equation stands out as a fundamental model in modern nonlinear science, governing the evolution of optical solitons. Considerable research determinations have been directed toward generalized forms of the NLS equation with constant coefficients, which serve as perfect models for examining complex wave dynamics [1–5]. These contain but are not limited to, the hyperbolic function method [6], the generalized Kudryashov method [7], the sub-ODE method [8], the extended improved tanh-function method [9], the anti-cubic law approach [10] the $(\frac{G'}{G^2})$-expansion method [11], the $\tan(\phi/2)$-expansion method [12], the simplest equation approach [13], variational iteration method [14], the unified method [15], the solitary wave ansatz method [16], the Riccati equation method [17], the auxiliary equation method [18], and several other advanced methods [19–22].

In current years, fractional differential equations (FDEs) have expanded significant attention due to their capacity to model an extensive spectrum of complex phenomena across many scientific and engineering disciplines. These contain fluid dynamics, geophysics, biological systems, acoustic dissipation, system identification, relaxation processes, signal and image processing, creep, economics, viscoelasticity, control theory, rheology, chaotic systems, and many others. While classical mechanics methods are typically valid to conservative systems, most real-world physical processes unveil non-conservative behavior. When the Lagrangian of a system is formulated using fractional derivatives, the resultant equations of motion more precisely capture non-conservative dynamics. Since several physical phenomena are essentially non-conservative, fractional-order differential equations afford a more effective modeling framework than traditional integer-order models. A major benefit of fractional derivatives lies in their ability to incorporate memory and hereditary properties of materials and processes. FDEs are particularly appropriate for modeling in discontinuous or heterogeneous media, where the fractional order replicates the fundamental fractal geometry of the system. Fractal structures, commonly encountered in physical and engineering perspectives, require advanced mathematical tools for exact representation. In this concern, local fractional calculus plays a vital role in characterizing such systems, particularly within Cantorian spaces [23–25].

An essential aspect of research in this field includes the development of both exact and numerical solutions to fractional differential equations. Several analytical and computational methods have been introduced to tackle these challenges. In particular, nonlinear fractional partial differential equations (FPDEs) work as powerful tools for modeling a range of nonlinear physical phenomena met in plasma physics, mathematical biology, solid-state physics, optical fiber systems, fluid mechanics, and chemical kinetics. Among the effective methods used for solving such equations is the fractional complex transform, which enables the conversion of FPDEs into their equivalent integer-order ordinary differential equations (ODEs). This method uses local fractional derivatives to transform fractal time-space domains into conventional continuous domains, thus enabling the application of classical solution methods and enhancing analytical tractability [26,27].

Over the last few years, research on fractional solitons has become an actively growing research area due to the capacity of fractional calculus to model phenomena that integer-order models cannot, like anomalous dispersion, hereditary memory, and fractal geometrical structures characteristic of most real-world systems. Researchers have increasingly utilized fractional-order models to analyze nonlinear wave dynamics in optical fibers, plasma physics, and hydrodynamic flows, where standard methods do not offer valid descriptions [28,29]. For example, fractional derivatives have been demonstrated to describe non-conservative processes with great accuracy, with resultant new forms of soliton solutions and stability conditions not found in integer-order formulations [30]. Further, recent studies have illustrated how fractional parameters can be used as effective tuning devices for modulating soliton amplitude, width, and velocity, providing useful benefits in engineering optical communication systems, plasma confinement systems, and energy transport processes [31]. These developments highlight the increasing significance of fractional soliton theory as a mathematical tool and as a source of technological innovation. In this regard, the current work makes a new contribution by using the newly developed mapping approach to the fractional (2+1)-dimensional Davey–Stewartson equation and, thus, obtaining a full family of soliton solutions. To the best of our knowledge, this is the first rational construction of such solutions for the given model, and the findings illustrate the way in which the fractional parameters radically change the dynamics of solitons with respect to traditional integer-order cases.

We utilize the local fractional derivative in this work in order to treat the fractional-order dynamics of the system. The local fractional derivative is applicable for non-differentiable functions and is ideal for simulating processes with fractal or locally discontinuous behavior. Its characteristics make it possible to use the fractional complex transform, which converts the fractional partial differential equation into an ordinary differential equation in a traveling-wave coordinate. This method maintains the indispensable fractional properties of the system and allows analytical solution techniques to be employed efficiently.

In this paper, we construct doubly periodic solutions for a recently proposed integrable fractional (2+1)-dimensional Davey–Stewartson (DS) equation [32] in terms of local fractional derivative and traveling wave solutions for the DS-type problem. These solutions are gained over the application of the mixed dn-sn method in conjunction with the fractional complex transform. The classical Davey–Stewartson equations, originally expressed by Davey and Stewartson, model the evolution of weakly nonlinear wave packets in shallow water and have been commonly developed in many branches of fluid dynamics.

The fractional (2+1)-dimensional DS equation under consideration is represented by Equation (1).

$$\begin{aligned} iD_t^{\alpha} p + a(D_x^{2\beta} p + D_y^{2\gamma} p) + b|p|^{2n} p - \lambda pq = 0, \\ D_x^{2\beta} q + D_y^{2\gamma} q + \delta D_x^{2\beta}(|p|^{2n}) = 0. \end{aligned} \tag{1}$$

In this case, the wave amplitude is represented by the complex-valued function $p = p(x, y, t)$, while the mean flow is represented by the real-valued function $q = q(x, y, t)$. $0 < \alpha \leq 1$, $0 < \beta \leq 1$, and $0 < \gamma \leq 1$ are satisfied by the parameters α, β, γ. The coefficients a, b, λ, and δ are also fixed and real valued. The power-law parameter linked to the nonlinearity of the system is shown by the exponent n. In Equation (1), the coupled structure describes the long-time evolution of a two-dimensional wave packet. This system is integrable in the strong sense and serves as an effective model in analyzing nonlinear wave dynamics.

Physically, the first equation controls the development of the wave packet amplitude $p(x,y,t)$ under the joint action of dispersion, nonlinearity, and interaction with the induced mean flow $q(x,y,t)$. The occurrence of the fractional temporal and spatial derivatives, D_t^{α}, $D_x^{2\beta}$, and $D_y^{2\gamma}$, accounts for memory effects, anomalous diffusion, and fractal geometrical structures common in complicated media like plasmas, density stratified fluids, and nonlinear optical media. These fractional derivatives generalize conventional integer-order dynamics with hereditary and nonlocal effects, thus presenting a more realistic model for non-conservative systems. The second equation is the self-consistent modification of the mean flow $q(x,y,t)$ to the developing wave packet.

The fractional Laplacian operators $D_x^{2\beta}q$ and $D_y^{2\gamma}q$ signal anomalous spatial diffusion of the background field, whereas the nonlinear source term $\delta D_x^{2\beta}\left(|p|^{2n}\right)$ describes the back-reaction of the intensity of the wave on the mean flow. Physically, this coupling mechanism prevents the evolution of p and q from becoming decoupled: the mean flow adjusts the wave packet dynamics, whereas the wave packet energy localized creates long-range modulations in the background field. Therefore, system (1) is a model of general form for characterizing the long-time dynamics of weakly nonlinear and weakly dispersive wave packets in multidimensional fractional media. It synthesizes the actions of nonlinearity, dispersion, nonlocal interactions, and fractional-order memory within one format, and, therefore, it is a useful tool for addressing nonlinear wave phenomenon in fluids, plasma physics, geophysical flows, and nonlinear optics. According to our knowledge, this is the first study to apply new mapping method to obtain the analytical solutions of the fractional (2+1)-DSE involving the local fractional derivative. The main motivation behind this research is to discover and construct solitary wave solutions for the fractional (2+1)-DSE model. This analytical methods have established to be active and useful tools to control such fractional-order nonlinear models [33,34].

The remainder of this paper is designed as follows: Section 2 outlines basic definitions and properties related to local fractional calculus. Section 3 details the algorithm method used to solve fractional partial differential equations via the fractional complex transform and methodology. In Section 4, the method applied to derive exact solutions for the fractional (2+1)-DSE equation. Result and discussion in Section 5 and, finally, Section 6 provides concluding remarks.

2. Preliminaries of Local Fractional Calculus and Methodology

2.1. Local Fractional Continuity of a Function

Definition 1. *If $h(r)$ is defined throughout some interval containing r_0 and all points near r_0 then $h(r)$ is called local fractional continuous at $r = r_0$, denoted by the following:*

$$\lim_{r \to r_0} h(r) = h(r_0),$$

There is a positive δ for every positive ϵ and some positive constant m, such that the following is true:

$$|h(r) - h(r_0)| < m\epsilon^{\beta}, \quad 0 < \beta \leq 1,$$

whenever $|r - r_0| < \delta$,δ,$\epsilon > 0$ and δ,$\epsilon \in \mathbb{R}$. Thus, on the interval (c,d), the function $h(r)$ is referred to as local fractional continuous, indicated by the following:

$$h(r) \in C_{\beta}(c,d),$$

the fractal dimension β has $0 < \beta \leq 1$.

Definition 2. *The Hölder function of exponent β is satisfied by the function $h(y) : \mathbb{R} \to \mathbb{R}, Y \mapsto h(Y)$, which is referred to as a nondifferentiable function of exponent β, $0 < \beta \leq 1$. We then have $a, b \in Y$.*

$$|h(a) - h(b)| \leq C|a - b|^{\beta}.$$

Definition 3. *A function $h(y) : \mathbb{R} \to \mathbb{R}, Y \mapsto h(Y)$ is called to be local fractional continuous of order β, $0 < \beta \leq 1$, or shortly β-local fractional continuous, when we have the following:*

$$h(y) - h(y_0) = O((y - y_0)^{\beta}).$$

Remark 1. *The space $C_{\beta}[c, d]$ is considered to include a function $h(r)$ if and only if it can be expressed as follows:*

$$h(r) - h(r_0) = O((r - r_0)^{\beta})$$

with any $r_0 \in [c, d]$ and $0 < \beta \leq 1$.

2.2. Local Fractional Derivative

Definition 4. *In $h(r) \in C_{\beta}(c, d)$, for a function $h(r)$ of order β at $r = r_0$, the local fractional derivative is defined as follows:*

$$h^{(\beta)}(r_0) = \left.\frac{d^{\beta}h(r)}{dr^{\beta}}\right|_{r=r_0} = \lim_{r \to r_0} \frac{\Delta^{\beta}(h(r) - h(r_0))}{(r - r_0)^{\beta}},$$

where $\Delta^{\beta}(h(r) - h(r_0)) \cong \Gamma(1 + \beta)(h(r) - h(r_0))$ and $0 < \beta \leq 1$.

Remark 2. *The following rules hold:*

$$\frac{d^{\beta}r^{m\beta}}{dr^{\beta}} = \frac{\Gamma(1 + m\beta)}{\Gamma(1 + (m - 1)\beta)} r^{(m-1)\beta};$$

and

$$\frac{d^{\beta}E_{\beta}(mr^{\beta})}{dr^{\beta}} = mE_{\beta}(mr^{\beta}), \quad m \text{ is a constant.}$$

Remark 3. *If $h(r) = (f \circ u)(r)$ where $u(r) = g(r)$, then we have the following:*

$$\frac{d^{\beta}h(r)}{dr^{\beta}} = f^{(\beta)}(g(r))\left(g^{(1)}(r)\right)^{\beta},$$

when $f^{(\beta)}(g(r))$ and $g^{(1)}(r)$ exist.

If $h(r) = (f \circ u)(r)$, where $u(r) = g(r)$, then we have the following:

$$\frac{d^{\beta}h(r)}{dr^{\beta}} = f^{(1)}(g(r))g^{(\beta)}(r),$$

when $f^{(1)}(g(r))$ and $g^{(\beta)}(x)$ exist.

3. Summary of New Mapping Method

The following steps define the new mapping method [35]:

1: Let us consider the fractional order differential equation which has the independent variable x, y and the dependent variable p and q.

$$F\left(p, q, D_t^{\alpha}p, D_t^{\beta}p, D_t^{\gamma}p, D_t^{\alpha}q, D_t^{\beta}q, D_t^{\gamma}q, p_x, D_x^{\alpha}p_x, D_x^{\beta}p_x, D_x^{\gamma}p_x, q_y, D_x^{\alpha}q_y, D_x^{\beta}q_y, D_x^{\gamma}q_y, \ldots\right) = 0, \tag{2}$$

Usually, F is a polynomial function of its argument and the dependent variable's subscripts indicate the partial derivatives.

2: We use the following traveling wave transformation for the fractional (2+1)-dimensional DS equations. A system of nonlinear ordinary differential equations is formed through the transformation of its exact solutions. Applying the following fractional complex transformation, we obtain the following:

$$p(x,y,t) = e^{i\theta}u(\eta), \qquad q(x,y,t) = v(\eta), \tag{3}$$

$$\theta = \frac{\theta_1 x^\beta}{\Gamma(1+\beta)} + \frac{\theta_2 y^\gamma}{\Gamma(1+\gamma)} + \frac{\theta_3 t^\alpha}{\Gamma(1+\alpha)} \; and \; \eta = \frac{\eta_1 x^\beta}{\Gamma(1+\beta)} + \frac{\eta_2 y^\gamma}{\Gamma(1+\gamma)} + \frac{\eta_3 t^\alpha}{\Gamma(1+\alpha)} \tag{4}$$

where $0 < \alpha, \beta, \gamma \leq 1$.

3: Putting Equation (3) and Equation (4) into Equation (2) yields an ordinary differential equation.

$$F(\theta, \alpha\theta', \alpha^2\theta'', \beta\theta', \beta^2\theta'', \gamma\theta', \gamma^2\theta'', ...) = 0, \tag{5}$$

4: This approach is predicated on the formal solution of Equation (2) existing as follows:

$$\theta(\eta) = \sum_{i=0}^{2N} c_i \psi^i(\eta), \tag{6}$$

where $\psi(\eta)$ satisfies the following:

$$\psi'^2(\eta) = f_0 + f_1\psi^2(\eta) + \frac{1}{2}f_2\psi^4(\eta) + \frac{1}{3}f_3\psi^6(\eta) \tag{7}$$

Here, c_i and f_j are constants, with $a_{2N} \neq 0$, where $N \in \mathbb{Z}^+$. Where N can be find by using homogeneous balancing rule.

5: By replacing Equation (5) with Equation (6) and Equation (7), a polynomial in $\psi(\eta)$ is obtained. A collection of nonlinear equations is obtained that can be resolved using the Mathematica to ascertain the unknown values of c_i, f_j, α, β and γ by combining all elements with similar powers and equating them to zero.

6: We substitute the values of c_i, f_j, α, β and γ as well as the solutions of Equation (5) listed in type-I and type-II, we have the exact solutions of Equation (2).

Type-I

Set 1: $f_1 < 0, f_2 > 0, f_3 = \frac{3f_2^2}{16f_1}, f_0 = \frac{16f_1^2}{27f_2}$,

$$\psi_1(\eta) = 4\sqrt{-\frac{f_1 \tanh^2(\eta\epsilon\sqrt{-\frac{f_1}{3}})}{3f_2\left(3 + \tanh^2(\eta\epsilon\sqrt{-\frac{f_1}{3}})\right)}}.$$

Set 2: $f_1 < 0, f_2 > 0, f_3 = \frac{3f_2^2}{16f_1}, f_0 = \frac{16f_1^2}{27f_2}$,

$$\psi_2(\eta) = 4\sqrt{-\frac{f_1 \coth^2(\eta\epsilon\sqrt{-\frac{f_1}{3}})}{3f_2\left(3 + \coth^2(\eta\epsilon\sqrt{-\frac{f_1}{3}})\right)}}.$$

Set 3: $f_1 > 0$, $f_3 = \frac{3f_2^2}{16f_1}$, $f_0 = 0$,

$$\psi_3(\eta) = \sqrt{-\frac{2f_1\left(1+\tanh\left(\eta\epsilon\sqrt{f_1}\right)\right)}{f_2}}.$$

Set 4: $f_1 > 0$, $f_3 = \frac{3f_2^2}{16f_1}$, $f_0 = 0$,

$$\psi_4(\eta) = \sqrt{-\frac{2f_1\left(1+\coth\left(\eta\epsilon\sqrt{f_1}\right)\right)}{f_2}}.$$

Set 5: $f_1 > 0$, $f_0 = 0$,

$$\psi_5(\eta) = \sqrt{-\frac{6f_1f_2\,\mathrm{sech}^2\left(\eta\sqrt{f_1}\right)}{3f_2^2 - 4f_1f_3\left(1+\epsilon\tanh^2\left(\eta\sqrt{f_1}\right)\right)}}.$$

Set 6: $f_1 > 0$, $f_0 = 0$,

$$\psi_6(\eta) = \sqrt{\frac{6f_1f_2\,\mathrm{csch}^2\left(\eta\sqrt{f_1}\right)}{3f_2^2 - 4f_1f_3\left(1+\epsilon\coth^2\left(\eta\sqrt{f_1}\right)\right)}}.$$

Set 7: $f_1 > 0$, $f_3 > 0$, $f_0 = 0$,

$$\psi_7(\eta) = \sqrt{-\frac{6f_1\,\mathrm{sech}^2\left(\eta\sqrt{f_1}\right)}{3f_2 + 4\epsilon\sqrt{3f_1f_3}\tanh\left(\eta\sqrt{f_1}\right)}}.$$

Set 8: $f_1 > 0$, $f_3 > 0$, $f_0 = 0$,

$$\psi_8(\eta) = \sqrt{\frac{6f_1\,\mathrm{csch}^2\left(\eta\sqrt{f_1}\right)}{3f_2 + 4\epsilon\sqrt{3f_1f_3}\coth\left(\eta\sqrt{f_1}\right)}}.$$

Set 9: $f_1 > 0$, $f_2 < 0$, $f_3 < 0$, $M > 0$, $f_0 = 0$,

$$\psi_9(\eta) = 2\sqrt{\frac{3f_1\,\mathrm{sech}^2\left(\eta\epsilon\sqrt{f_1}\right)}{2\sqrt{M} - \left(\sqrt{M}+3f_2\right)\mathrm{sech}^2\left(\eta\epsilon\sqrt{f_1}\right)}}.$$

Set 10: $f_1 > 0$, $f_2 < 0$, $f_3 < 0$, $M > 0$, $f_0 = 0$,

$$\psi_{10}(\eta) = 2\sqrt{\frac{3f_1\,\mathrm{csch}^2\left(\eta\epsilon\sqrt{f_1}\right)}{2\sqrt{M} + \left(\sqrt{M}+3f_2\right)\mathrm{csch}^2\left(\eta\epsilon\sqrt{f_1}\right)}}.$$

Set 11: $f_1 > 0$, $M > 0$, $f_0 = 0$,

$$\psi_{11}(\eta) = 2\sqrt{\frac{3f_1}{\epsilon\sqrt{M}\cosh\left(2\sqrt{f_1}\eta\right) - 3f_2}}.$$

Set 12: $f_1 > 0$, $M < 0$, $f_0 = 0$,

$$\psi_{12}(\eta) = 2\sqrt{\frac{3f_1}{\epsilon\sqrt{-M}\sinh\left(2\sqrt{f_1}\eta\right) - 3f_2}},$$

where $M = 9f_2^2 - 48f_1f_3$ and $\epsilon = \pm 1$.

Type-II

Set 13: $f_1 > 0$, $f_2 < 0$, $f_3 = \frac{3f_2^2}{16f_1}$, $f_0 = \frac{16f_1^2}{27f_2}$,

$$\psi_{13}(\eta) = 4\sqrt{\frac{f_1 \tan^2\left(\epsilon\eta\sqrt{\frac{f_1}{3}}\right)}{3f_2\left(3 - \tan^2\left(\epsilon\eta\sqrt{\frac{f_1}{3}}\right)\right)}}.$$

Set 14: $f_1 > 0$, $f_2 < 0$, $f_3 = \frac{3f_2^2}{16f_1}$, $f_0 = \frac{16f_1^2}{27f_2}$,

$$\psi_{14}(\eta) = 4\sqrt{\frac{f_1 \cot^2\left(\epsilon\eta\sqrt{\frac{f_1}{3}}\right)}{3f_2\left(3 - \cot^2\left(\epsilon\eta\sqrt{\frac{f_1}{3}}\right)\right)}}.$$

Set 15: $f_1 < 0$, $f_3 > 0$, $f_0 = 0$,

$$\psi_{15}(\eta) = \sqrt{-\frac{6f_1 \sec^2\left(\eta\sqrt{-f_1}\right)}{3f_2 + 4\epsilon\sqrt{-3f_1f_3}\tan\left(\eta\sqrt{-f_1}\right)}}.$$

Set 16: $f_1 < 0$, $f_3 > 0$, $f_0 = 0$,

$$\psi_{16}(\eta) = \sqrt{-\frac{6f_1 \csc^2\left(\eta\sqrt{-f_1}\right)}{3f_2 + 4\epsilon\sqrt{-3f_1f_3}\cot\left(\eta\sqrt{-f_1}\right)}}.$$

Set 17: $f_1 < 0$, $f_2 > 0$, $f_3 < 0$, $M > 0$, $f_0 = 0$,

$$\psi_{17}(\eta) = 2\sqrt{-\frac{3f_1 \sec^2\left(\epsilon\eta\sqrt{-f_1}\right)}{2\sqrt{M} - \left(\sqrt{M} - 3f_2\right)\sec^2\left(\epsilon\eta\sqrt{-f_1}\right)}}.$$

Set 18: $f_1 < 0$, $f_2 > 0$, $f_3 < 0$, $M > 0$, $f_0 = 0$,

$$\psi_{18}(\eta) = 2\sqrt{\frac{3f_1 \csc^2\left(\epsilon\eta\sqrt{-f_1}\right)}{2\sqrt{M} - \left(3f_2 + \sqrt{M}\right)\csc^2\left(\epsilon\eta\sqrt{-f_1}\right)}}.$$

Set 19: $f_1 < 0$, $M > 0$, $f_0 = 0$,

$$\psi_{19}(\eta) = 2\sqrt{\frac{3f_1}{-3f_2 + \epsilon\sqrt{M}\cos\left(2\eta\sqrt{-f_1}\right)}}.$$

Set 20: $f_1 < 0$, $M > 0$, $f_0 = 0$,

$$\psi_{20}(\eta) = 2\sqrt{\frac{3f_1}{-3f_2 + \epsilon\sqrt{M}\sin\left(2\eta\sqrt{-f_1}\right)}},$$

where $M = 9f_2^2 - 48f_1f_3$ and $\epsilon = \pm 1$.

4. Fractional (2+1)-Dimensional Davey–Stewartson Equation and Methodology

4.1. Fractional (2+1)-Dimensional Davey–Stewartson Equation

For the fractional (2+1)-dimensional DS Equation (1), we first obtain the exact solutions. A system of nonlinear ordinary differential equations is formed through the transformation of its exact solutions. Applying the following fractional complex transformation, we obtain the following:

$$p(x,y,t) = e^{i\theta}u(\eta), \qquad q(x,y,t) = v(\eta), \tag{8}$$

$$\theta = \frac{\theta_1 x^\beta}{\Gamma(1+\beta)} + \frac{\theta_2 y^\gamma}{\Gamma(1+\gamma)} + \frac{\theta_3 t^\alpha}{\Gamma(1+\alpha)} \; and \; \eta = \frac{\eta_1 x^\beta}{\Gamma(1+\beta)} + \frac{\eta_2 y^\gamma}{\Gamma(1+\gamma)} + \frac{\eta_3 t^\alpha}{\Gamma(1+\alpha)} \tag{9}$$

Equation (1) reduced to the coupled nonlinear ODE is as follows:

$$-(\theta_3 + a\theta_1^2 + a\theta_2^2)u + (a\eta_1^2 + a\eta_2^2)u_{\eta\eta} + bu^{2n+1} - \lambda uv = 0, \tag{10}$$

$$\eta_1^2 v_{\eta\eta} + \eta_2^2 v_{\eta\eta} + \delta\eta_1^2 (u^{2n})_{\eta\eta} = 0. \tag{11}$$

The value of η_3 is set to $-2a\eta_1\theta_1 - 2a\eta_2\theta_2$. Then with respect to η, Equation (11) is integrated twice term by term with integration constants taken to be zero. In integrating Equation (11) to obtain Equation (12), the integration constants are set to zero to derive physically localized soliton solutions that vanish at infinity. This choice does not affect the underlying physics, as nonzero constants would only shift the solution or add a trivial background without producing fundamentally new soliton structures. So we obtain the following:

$$v = -\frac{\delta\eta_1^2 u^{2n}}{\eta_1^2 + \eta_2^2}. \tag{12}$$

Using Equation (12) into Equation (10) yields the following:

$$-(\theta_3 + a\theta_1^2 + a\theta_2^2)u + (a\eta_1^2 + a\eta_2^2)u_{\eta\eta} + bu^{2n+1} + \lambda\frac{\delta\eta_1^2 u^{2n+1}}{\eta_1^2 + \eta_2^2} = 0. \tag{13}$$

By using the transformation as follows:

$$u(\eta) = \Phi^{\frac{1}{n}}(\eta),$$

Now solve Equation (13) which is further reduced to the following:

$$-(\theta_3 + a\theta_1^2 + a\theta_2^2)n^2\Phi^2 + (a\eta_1^2 + a\eta_2^2)(1-n)\Phi_\eta^2 + (a\eta_1^2 + a\eta_2^2)n\Phi\Phi_{\eta\eta} + bn^2\Phi^4 + \lambda\frac{\delta\eta_1^2 n^2\Phi^4}{\eta_1^2 + \eta_2^2} = 0. \tag{14}$$

Here, we use the local fractional derivative to solve the fractional-order (2+1)-dimensional Davey–Stewartson equation. To make the fractional partial differential equation turn into an ordinary differential equation, we use the fractional complex transform in Equations (8) and (9), which adds a traveling-wave coordinate η and a phase function θ in terms of the fractional orders α, β, γ. The characteristics of the local fractional derivative, such as linearity, the chain rule (Remark 3), and the power and Mittag–Leffler functions' derivative (Remark 2), enable this transformation to reduce fractional derivatives in x, y, and t to ordinary derivatives with respect to η. This process retains the key frac-

tional dynamics while projecting the governing PDE to coupled nonlinear ODE system in Equations (10) and (11), simplified further to Equation (14) for the construction of analytical solutions.

4.2. Solutions to Fractional (2+1)-Dimensional Davey-Stewartson Equation Using NMM

In this part, we investigate a method known as NMM to investigate the exact solution of (2+1)-dimensional DS equation. We obtain $N = 1$ by applying the balancing principle in Equation (14). Then, Equation (6) is as follows:

$$\theta(\eta) = c_0 + c_1\psi(\eta) + c_2\psi^2(\eta). \tag{15}$$

We obtain an algebraic equation system by equating the factors of $\psi(\eta)$ to zero and placing Equation (15) into Equation (7).The coefficients of like power of $\psi(\eta)$ are then set to zero, resulting in the following algebraic form:

$\psi(\eta)^0$ coeff.:

$$\begin{aligned} &ac_1^2f_0\eta_1^2 + ac_1^2f_0\eta_2^2 + 2ac_2c_0f_0\eta_1^2n + 2ac_2c_0f_0\eta_2^2n - ac_1^2f_0\eta_1^2n \\ &-ac_1^2f_0\eta_2^2n - ac_0^2\theta_1^2n^2 - ac_0^2\theta_2^2n^2 + bc_0^4n^2 + \frac{c_0^4\delta\eta_1^2\lambda n^2}{\eta_1^2+\eta_2^2} - c_0^2\theta_3n^2 = 0, \end{aligned}$$

$\psi(\eta)^1$ coeff.:

$$\begin{aligned} &4ac_1c_2f_0\eta_1^2 + 4ac_1c_2f_0\eta_2^2 + ac_1c_0f_1\eta_1^2n + ac_1c_0f_1\eta_2^2n - 2ac_1c_2f_0\eta_1^2n - 2ac_1c_2f_0\eta_2^2n \\ &-2ac_1c_0\theta_1^2n^2 - 2ac_1c_0\theta_2^2n^2 + 4bc_1c_0^3n^2 + \frac{4c_1c_0^3\delta\eta_1^2\lambda n^2}{\eta_1^2+\eta_2^2} - 2c_1c_0\theta_3n^2 = 0, \end{aligned}$$

$\psi(\eta)^2$ coeff.:

$$\begin{aligned} &4ac_2^2f_0\eta_1^2 + ac_1^2f_1\eta_1^2 + 4ac_2^2f_0\eta_2^2 + ac_1^2f_1\eta_2^2 + 4ac_2c_0f_1\eta_1^2n + 4ac_2c_0f_1\eta_2^2n \\ &-2ac_2^2f_0\eta_1^2n - 2ac_2^2f_0\eta_2^2n - 2ac_2c_0\theta_1^2n^2 - 2ac_2c_0\theta_2^2n^2 - ac_1^2\theta_1^2n^2 - ac_1^2\theta_2^2n^2 \\ &+4bc_2c_0^3n^2 + 6bc_1^2c_0^2n^2 + \frac{4c_2c_0^3\delta\eta_1^2\lambda n^2}{\eta_1^2+\eta_2^2} + \frac{6c_1^2c_0^2\delta\eta_1^2\lambda n^2}{\eta_1^2+\eta_2^2} - 2c_2c_0\theta_3n^2 - c_1^2\theta_3n^2 = 0, \end{aligned}$$

$\psi(\eta)^3$ coeff.:

$$\begin{aligned} &4ac_2c_1f_1\eta_1^2 + 4ac_2c_1f_1\eta_2^2 + ac_2c_1f_1\eta_1^2n + ac_0c_1f_2\eta_1^2n + ac_2c_1f_1\eta_2^2n \\ &+ac_0c_1f_2\eta_2^2n - 2ac_2c_1\theta_1^2n^2 - 2ac_2c_1\theta_2^2n^2 + 4bc_0c_1^3n^2 + 12bc_0^2c_2c_1n^2 \\ &+\frac{4c_0c_1^3\delta\eta_1^2\lambda n^2}{\eta_1^2+\eta_2^2} + \frac{12c_0^2c_2c_1\delta\eta_1^2\lambda n^2}{\eta_1^2+\eta_2^2} - 2c_2c_1\theta_3n^2 = 0, \end{aligned}$$

$\psi(\eta)^4$ coeff.:

$$\begin{aligned} &\frac{1}{2}ac_1^2f_2\eta_1^2 + \frac{1}{2}ac_1^2f_2\eta_2^2 + 4ac_2^2f_1\eta_1^2 + 4ac_2^2f_1\eta_2^2 + \frac{1}{2}ac_1^2f_2\eta_1^2n + \frac{1}{2}ac_1^2f_2\eta_2^2n \\ &+3ac_0c_2f_2\eta_1^2n + 3ac_0c_2f_2\eta_2^2n - ac_2^2\theta_1^2n^2 - ac_2^2\theta_2^2n^2 + bc_1^4n^2 + 12bc_0c_2c_1^2n^2 \\ &+6bc_0^2c_2^2n^2 + \frac{c_1^4\delta\eta_1^2\lambda n^2}{\eta_1^2+\eta_2^2} + \frac{12c_0c_2c_1^2\delta\eta_1^2\lambda n^2}{\eta_1^2+\eta_2^2} + \frac{6c_0^2c_2^2\delta\eta_1^2\lambda n^2}{\eta_1^2+\eta_2^2} - c_2^2\theta_3n^2 = 0, \end{aligned}$$

$\psi(\eta)^5$ coeff.:

$$2ac_2c_1f_2\eta_1^2 + 2ac_2c_1f_2\eta_2^2 + 2ac_2c_1f_2\eta_1^2 n + ac_0c_1f_3\eta_1^2 n + 2ac_2c_1f_2\eta_2^2 n$$
$$+ac_0c_1f_3\eta_2^2 n + 4bc_2c_1^3 n^2 + 12bc_0c_2^2c_1 n^2 + \frac{4c_2c_1^3\delta\eta_1^2\lambda n^2}{\eta_1^2+\eta_2^2} + \frac{12c_0c_2^2c_1\delta\eta_1^2\lambda n^2}{\eta_1^2+\eta_2^2} = 0,$$

$\psi(\eta)^6$ coeff.:

$$2ac_2^2f_2\eta_1^2 + 2ac_2^2f_2\eta_2^2 + \frac{1}{3}ac_1^2f_3\eta_1^2 + \frac{1}{3}ac_1^2f_3\eta_2^2 + ac_2^2f_2\eta_1^2 n + ac_2^2f_2\eta_2^2 n + \frac{8}{3}ac_0c_2f_3\eta_1^2 n$$
$$+\frac{8}{3}ac_0c_2f_3\eta_2^2 n + \frac{2}{3}ac_1^2f_3\eta_1^2 n + \frac{2}{3}ac_1^2f_3\eta_2^2 n + 4bc_0c_2^3 n^2 + 6bc_1^2c_2^2 n^2$$
$$+\frac{4c_0c_2^3\delta\eta_1^2\lambda n^2}{\eta_1^2+\eta_2^2} + \frac{6c_1^2c_2^2\delta\eta_1^2\lambda n^2}{\eta_1^2+\eta_2^2} = 0,$$

$\psi(\eta)^7$ coeff.:

$$\frac{4}{3}ac_1c_2f_3\eta_1^2 + \frac{4}{3}ac_1c_2f_3\eta_2^2 + \frac{7}{3}ac_1c_2f_3\eta_1^2 n + \frac{7}{3}ac_1c_2f_3\eta_2^2 n + 4bc_1c_2^3 n^2 + \frac{4c_1c_2^3\delta\eta_1^2\lambda n^2}{\eta_1^2+\eta_2^2} = 0,$$

$\psi(\eta)^8$ coeff.:

$$\frac{4}{3}ac_2^2f_3\eta_1^2 + \frac{4}{3}ac_2^2f_3\eta_2^2 + \frac{4}{3}ac_2^2f_3\eta_1^2 n + \frac{4}{3}ac_2^2f_3\eta_2^2 n + bc_2^4 n^2 + \frac{c_2^4\delta\eta_1^2\lambda n^2}{\eta_1^2+\eta_2^2} = 0.$$

The following several solutions can be obtained by solving the mentioned set of equations using Mathematica software 12.3.

$$c_0 = \frac{\sqrt{\eta_1^2+\eta_2^2}\sqrt{n+1}\sqrt{a\theta_1^2+a\theta_2^2+\theta_3}}{\sqrt{b\eta_1^2+b\eta_2^2+\delta\eta_1^2\lambda}},\ c_1 = 0,$$
$$f_0 = -\frac{n^2\sqrt{n+1}(a\theta_1^2+a\theta_2^2+\theta_3)^{3/2}}{2ac_2\sqrt{\eta_1^2+\eta_2^2}\sqrt{\eta_1^2(b+\delta\lambda)+b\eta_2^2}},\ f_1 = -\frac{5n^2(a\theta_1^2+a\theta_2^2+\theta_3)}{4a(\eta_1^2+\eta_2^2)},$$
$$f_2 = \frac{2c_2n^2\sqrt{a\theta_1^2+a\theta_2^2+\theta_3}\sqrt{\eta_1^2(b+\delta\lambda)+b\eta_2^2}}{a(\eta_1^2+\eta_2^2)^{3/2}\sqrt{n+1}},\ f_3 = -\frac{3c_2^2n^2(b\eta_1^2+b\eta_2^2+\delta\eta_1^2\lambda)}{4a(\eta_1^2+\eta_2^2)^2(n+1)}.$$

The (2+1)-DSE provided in Equation (14) has the following exact solutions obtained using the values mentioned above.

Type 1

Set 1: If $f_1 < 0$, $f_2 > 0$, $f_3 = \frac{3f_2^2}{16f_1}$ and $f_0 = \frac{16f_1^2}{27f_2}$, then we have dark soliton solutions

$$p_1(x,y,t) = \frac{e^{i\theta}\left(-16c_2f_1\tanh^2\left(\frac{\sqrt{-f_1}\eta\epsilon}{\sqrt{3}}\right) + 3c_0f_2\tanh^2\left(\frac{\sqrt{-f_1}\eta\epsilon}{\sqrt{3}}\right) + 9c_0f_2\right)}{3f_2\left(\tanh^2\left(\frac{\sqrt{-f_1}\eta\epsilon}{\sqrt{3}}\right)+3\right)},$$

$$q_1(x,y,t) = \frac{\delta\eta_1^2\left(-16c_2f_1\tanh^2\left(\frac{\sqrt{-f_1}\eta\epsilon}{\sqrt{3}}\right) + 3c_0f_2\tanh^2\left(\frac{\sqrt{-f_1}\eta\epsilon}{\sqrt{3}}\right) + 9c_0f_2\right)^2}{9f_2^2(\eta_1^2+\eta_2^2)\left(\tanh^2\left(\frac{\sqrt{-f_1}\eta\epsilon}{\sqrt{3}}\right)+3\right)^2}.$$

Set 2: If $f_1 < 0$, $f_2 > 0$, $f_3 = \frac{3f_2^2}{16f_1}$ and $f_0 = \frac{16f_1^2}{27f_2}$, then we have the singular soliton solutions as follows:

$$p_2(x,y,t) = \frac{e^{i\theta}\left(-16c_2f_1\coth^2\left(\frac{\sqrt{-f_1}\eta\epsilon}{\sqrt{3}}\right)+3c_0f_2\coth^2\left(\frac{\sqrt{-f_1}\eta\epsilon}{\sqrt{3}}\right)+9c_0f_2\right)}{3f_2\left(\coth^2\left(\frac{\sqrt{-f_1}\eta\epsilon}{\sqrt{3}}\right)+3\right)},$$

$$q_2(x,y,t) = \frac{\delta\eta_1^2\left(-16c_2f_1\coth^2\left(\frac{\sqrt{-f_1}\eta\epsilon}{\sqrt{3}}\right)+3c_0f_2\coth^2\left(\frac{\sqrt{-f_1}\eta\epsilon}{\sqrt{3}}\right)+9c_0f_2\right)^2}{9f_2^2(\eta_1^2+\eta_2^2)\left(\coth^2\left(\frac{\sqrt{-f_1}\eta\epsilon}{\sqrt{3}}\right)+3\right)^2}.$$

For the coefficients, $c_0 = \frac{\sqrt{\eta_1^2+\eta_2^2}\sqrt{n+1}\sqrt{a\theta_1^2+a\theta_2^2+\theta_3}}{\sqrt{b\eta_1^2+b\eta_2^2+\delta\eta_1^2\lambda}}$, $c_1 = 0$, $f_1 = -\frac{5n^2\left(a\theta_1^2+a\theta_2^2+\theta_3\right)}{4a\left(\eta_1^2+\eta_2^2\right)}$, $f_2 = \frac{2c_2n^2\sqrt{a\theta_1^2+a\theta_2^2+\theta_3}\sqrt{\eta_1^2(b+\delta\lambda)+b\eta_2^2}}{a\left(\eta_1^2+\eta_2^2\right)^{3/2}\sqrt{n+1}}$, $f_3 = -\frac{3c_2^2n^2\left(b\eta_1^2+b\eta_2^2+\delta\eta_1^2\lambda\right)}{4a\left(\eta_1^2+\eta_2^2\right)^2(n+1)}$.

Set 3: If $f_1 > 0$, $f_3 = \frac{3f_2^2}{16f_1}$ and $f_0 = 0$, then we have the dark soliton solutions as follows:

$$p_3(x,y,t) = \frac{e^{i\theta}\left(-2c_2f_1\tanh\left(\sqrt{f_1}\eta\epsilon\right)-2c_2f_1+c_0f_2\right)}{f_2},$$

$$q_3(x,y,t) = \frac{\delta\eta_1^2\left(-2c_2f_1\tanh\left(\sqrt{f_1}\eta\epsilon\right)-2c_2f_1+c_0f_2\right)^2}{f_2^2(\eta_1^2+\eta_2^2)}.$$

Set 4: If $f_1 > 0$, $f_3 = \frac{3f_2^2}{16f_1}$ and $f_0 = 0$, then we have the singular soliton solutions as follows:

$$p_4(x,y,t) = \frac{e^{i\theta}\left(-2c_2f_1\coth\left(\sqrt{f_1}\eta\epsilon\right)-2c_2f_1+c_0f_2\right)}{f_2},$$

$$q_4(x,y,t) = \frac{\delta\eta_1^2\left(-2c_2f_1\coth\left(\sqrt{f_1}\eta\epsilon\right)-2c_2f_1+c_0f_2\right)^2}{f_2^2(\eta_1^2+\eta_2^2)}.$$

Set 5: If $f_1 > 0$ and $f_0 = 0$, then we have the combo bright-dark soliton solutions as follows:

$$p_5(x,y,t) = e^{i\theta}\left(c_0 - \frac{6c_2f_1f_2\mathrm{sech}^2\left(\sqrt{f_1}\eta\right)}{3f_2^2-4f_1f_3\left(\epsilon\tanh^2\left(\sqrt{f_1}\eta\right)+1\right)}\right),$$

$$q_5(x,y,t) = \frac{\delta\eta_1^2\left(c_0 - \frac{6c_2f_1f_2\mathrm{sech}^2\left(\sqrt{f_1}\eta\right)}{3f_2^2-4f_1f_3\left(\epsilon\tanh^2\left(\sqrt{f_1}\eta\right)+1\right)}\right)^2}{\eta_1^2+\eta_2^2}.$$

Set 6: If $f_1 > 0$ and $f_0 = 0$, then we have the singular soliton solutions as follows:

$$p_6(x,y,t) = e^{i\theta}\left(\frac{6c_2f_1f_2\mathrm{csch}^2\left(\sqrt{f_1}\eta\right)}{3f_2^2-4f_1f_3\left(\epsilon\coth^2\left(\sqrt{f_1}\eta\right)+1\right)}+c_0\right),$$

$$q_6(x,y,t) = \frac{\delta\eta_1^2\left(\frac{6c_2f_1f_2\operatorname{csch}^2\left(\sqrt{f_1}\eta\right)}{3f_2^2-4f_1f_3\left(\epsilon\coth^2\left(\sqrt{f_1}\eta\right)+1\right)}+c_0\right)^2}{\eta_1^2+\eta_2^2}.$$

Set 7: If $f_1 > 0$, $f_3 > 0$ and $f_0 = 0$, then we have the combo bright-dark soliton solutions as follows:

$$p_7(x,y,t) = \frac{e^{i\theta}\left(-6c_2f_1\operatorname{sech}^2(\sqrt{f_1}\eta)+4\sqrt{3}c_0\sqrt{f_1f_3}\epsilon\tanh(\sqrt{f_1}\eta)+3c_0f_2\right)}{4\sqrt{3}\sqrt{f_1f_3}\epsilon\tanh(\sqrt{f_1}\eta)+3f_2},$$

$$q_7(x,y,t) = \frac{\delta\eta_1^2\left(-6c_2f_1\operatorname{sech}^2(\sqrt{f_1}\eta)+4\sqrt{3}c_0\sqrt{f_1f_3}\epsilon\tanh(\sqrt{f_1}\eta)+3c_0f_2\right)^2}{(\eta_1^2+\eta_2^2)\left(4\sqrt{3}\sqrt{f_1f_3}\epsilon\tanh(\sqrt{f_1}\eta)+3f_2\right)^2}.$$

Set 8: If $f_1 > 0$, $f_3 > 0$ and $f_0 = 0$, the we have singular soliton solutions as follows:

$$p_8(x,y,t) = \frac{e^{i\theta}\left(6c_2f_1\operatorname{csch}^2(\sqrt{f_1}\eta)+4\sqrt{3}c_0\sqrt{f_1f_3}\epsilon\coth(\sqrt{f_1}\eta)+3c_0f_2\right)}{4\sqrt{3}\sqrt{f_1f_3}\epsilon\coth(\sqrt{f_1}\eta)+3f_2},$$

$$q_8(x,y,t) = \frac{\delta\eta_1^2\left(6c_2f_1\operatorname{csch}^2(\sqrt{f_1}\eta)+4\sqrt{3}c_0\sqrt{f_1f_3}\epsilon\coth(\sqrt{f_1}\eta)+3c_0f_2\right)^2}{(\eta_1^2+\eta_2^2)\left(4\sqrt{3}\sqrt{f_1f_3}\epsilon\coth(\sqrt{f_1}\eta)+3f_2\right)^2}.$$

Set 9: If $f_1 > 0$, $f_2 < 0$, $f_3 < 0$, $M > 0$ and $f_0 = 0$, then we have the bright soliton solutions as follows:

$$p_9(x,y,t) = e^{i\theta}\left(\frac{12c_2f_1\operatorname{sech}^2(\sqrt{f_1}\eta\epsilon)}{2\sqrt{M}-\left(3f_2+\sqrt{M}\right)\operatorname{sech}^2(\sqrt{f_1}\eta\epsilon)}+c_0\right),$$

$$q_9(x,y,t) = \frac{\delta\eta_1^2\left(\frac{12c_2f_1\operatorname{sech}^2\left(\sqrt{f_1}\eta\epsilon\right)}{2\sqrt{M}-\left(3f_2+\sqrt{M}\right)\operatorname{sech}^2\left(\sqrt{f_1}\eta\epsilon\right)}+c_0\right)^2}{\eta_1^2+\eta_2^2}.$$

Set 10: If $f_1 > 0$, $f_2 < 0$, $f_3 < 0$, $M > 0$ and $f_0 = 0$, then we have the singular soliton solutions as follows:

$$p_{10}(x,y,t) = e^{i\theta}\left(\frac{12c_2f_1\operatorname{csch}^2(\sqrt{f_1}\eta\epsilon)}{\left(\sqrt{M}-3f_2\right)\operatorname{csch}^2(\sqrt{f_1}\eta\epsilon)+2\sqrt{M}}+c_0\right),$$

$$q_{10}(x,y,t) = \frac{\delta\eta_1^2\left(\frac{12c_2f_1\operatorname{csch}^2\left(\sqrt{f_1}\eta\epsilon\right)}{\left(\sqrt{M}-3f_2\right)\operatorname{csch}^2\left(\sqrt{f_1}\eta\epsilon\right)+2\sqrt{M}}+c_0\right)^2}{\eta_1^2+\eta_2^2}.$$

Set 11: If $f_1 > 0$, $M > 0$ and $f_0 = 0$, then we have singular soliton solutions as follows:

$$p_{11}(x,y,t) = e^{i\theta}\left(\frac{12c_2f_1}{\sqrt{M}\epsilon\cosh(2\sqrt{f_1}\eta)-3f_2}+c_0\right),$$

$$q_{11}(x,y,t) = \frac{\delta\eta_1^2\left(\frac{12c_2f_1}{\sqrt{M}\epsilon\cosh\left(2\sqrt{f_1}\eta\right)-3f_2}+c_0\right)^2}{\eta_1^2+\eta_2^2}.$$

Set 12: If $f_1 > 0$, $M < 0$ and $f_0 = 0$, then we have the singular soliton solutions as follows:

$$p_{12}(x,y,t) = e^{i\theta}\left(\frac{12c_2f_1}{\sqrt{-M}\epsilon\sinh\left(2\sqrt{f_1}\eta\right) - 3f_2} + c_0\right),$$

$$q_{12}(x,y,t) = \frac{\delta\eta_1^2\left(\frac{12c_2f_1}{\sqrt{-M}\epsilon\sinh\left(2\sqrt{f_1}\eta\right)-3f_2} + c_0\right)^2}{\eta_1^2+\eta_2^2}.$$

Type 2

Set 13: If $f_1 > 0$, $f_2 < 0$, $f_3 = \frac{3f_2^2}{16f_1}$ and $f_0 = \frac{16f_1^2}{27f_2}$, then we have periodic soliton solutions as follows:

$$p_{13}(x,y,t) = \frac{e^{i\theta}\left(-16c_2f_1\tan^2\left(\frac{\sqrt{f_1}\eta\epsilon}{\sqrt{3}}\right) + 3c_0f_2\tan^2\left(\frac{\sqrt{f_1}\eta\epsilon}{\sqrt{3}}\right) - 9c_0f_2\right)}{3f_2\left(\tan^2\left(\frac{\sqrt{f_1}\eta\epsilon}{\sqrt{3}}\right) - 3\right)},$$

$$q_{13}(x,y,t) = \frac{\delta\eta_1^2\left(-16c_2f_1\tan^2\left(\frac{\sqrt{f_1}\eta\epsilon}{\sqrt{3}}\right) + 3c_0f_2\tan^2\left(\frac{\sqrt{f_1}\eta\epsilon}{\sqrt{3}}\right) - 9c_0f_2\right)^2}{9f_2^2(\eta_1^2+\eta_2^2)\left(\tan^2\left(\frac{\sqrt{f_1}\eta\epsilon}{\sqrt{3}}\right) - 3\right)^2}.$$

Set 14: If $f_1 > 0$, $f_2 < 0$, $f_3 = \frac{3f_2^2}{16f_1}$ and $f_0 = \frac{16f_1^2}{27f_2}$, then we have the periodic soliton solutions as follows:

$$p_{14}(x,y,t) = \frac{e^{i\theta}\left(-16c_2f_1\cot^2\left(\frac{\sqrt{f_1}\eta\epsilon}{\sqrt{3}}\right) + 3c_0f_2\cot^2\left(\frac{\sqrt{f_1}\eta\epsilon}{\sqrt{3}}\right) - 9c_0f_2\right)}{3f_2\left(\cot^2\left(\frac{\sqrt{f_1}\eta\epsilon}{\sqrt{3}}\right) - 3\right)},$$

$$q_{14}(x,y,t) = \frac{\delta\eta_1^2\left(-16c_2f_1\cot^2\left(\frac{\sqrt{f_1}\eta\epsilon}{\sqrt{3}}\right) + 3c_0f_2\cot^2\left(\frac{\sqrt{f_1}\eta\epsilon}{\sqrt{3}}\right) - 9c_0f_2\right)^2}{9f_2^2(\eta_1^2+\eta_2^2)\left(\cot^2\left(\frac{\sqrt{f_1}\eta\epsilon}{\sqrt{3}}\right) - 3\right)^2}.$$

Set 15: If $f_1 < 0$, $f_3 > 0$ and $f_0 = 0$, then we have the periodic soliton solutions as follows:

$$p_{15}(x,y,t) = \frac{e^{i\theta}\left(-6c_2f_1\sec^2\left(\sqrt{-f_1}\eta\right) + 4\sqrt{3}c_0\sqrt{-f_1f_3}\epsilon\tan\left(\sqrt{-f_1}\eta\right) + 3c_0f_2\right)}{4\sqrt{3}\sqrt{-f_1f_3}\epsilon\tan\left(\sqrt{-f_1}\eta\right) + 3f_2},$$

$$q_{15}(x,y,t) = \frac{\delta\eta_1^2\left(-6c_2f_1\sec^2\left(\sqrt{-f_1}\eta\right) + 4\sqrt{3}c_0\sqrt{-f_1f_3}\epsilon\tan\left(\sqrt{-f_1}\eta\right) + 3c_0f_2\right)^2}{(\eta_1^2+\eta_2^2)\left(4\sqrt{3}\sqrt{-f_1f_3}\epsilon\tan\left(\sqrt{-f_1}\eta\right) + 3f_2\right)^2}.$$

Set 16: If $f_1 < 0$, $f_3 > 0$ and $f_0 = 0$, then we have the periodic soliton solutions as follows:

$$p_{16}(x,y,t) = \frac{e^{i\theta}\left(-6c_2f_1\csc^2\left(\sqrt{-f_1}\eta\right) + 4\sqrt{3}c_0\sqrt{-f_1f_3}\epsilon\cot\left(\sqrt{-f_1}\eta\right) + 3c_0f_2\right)}{4\sqrt{3}\sqrt{-f_1f_3}\epsilon\cot\left(\sqrt{-f_1}\eta\right) + 3f_2},$$

$$q_{16}(x,y,t)=\frac{\delta\eta_1^2\left(-6c_2f_1\csc^2\left(\sqrt{-f_1}\eta\right)+4\sqrt{3}c_0\sqrt{-f_1f_3}\epsilon\cot\left(\sqrt{-f_1}\eta\right)+3c_0f_2\right)^2}{\left(\eta_1^2+\eta_2^2\right)\left(4\sqrt{3}\sqrt{-f_1f_3}\epsilon\cot\left(\sqrt{-f_1}\eta\right)+3f_2\right)^2}.$$

Set 17: If $f_1<0$, $f_2>0$, $f_3<0$, $M>0$ and $f_0=0$, then we have the periodic soliton solutions as follows:

$$p_{17}(x,y,t)=e^{i\theta}\left(c_0-\frac{12c_2f_1\sec^2\left(\sqrt{-f_1}\eta\epsilon\right)}{2\sqrt{M}-\left(\sqrt{M}-3f_2\right)\sec^2\left(\sqrt{-f_1}\eta\epsilon\right)}\right),$$

$$q_{17}(x,y,t)=\frac{\delta\eta_1^2\left(c_0-\frac{12c_2f_1\sec^2\left(\sqrt{-f_1}\eta\epsilon\right)}{2\sqrt{M}-\left(\sqrt{M}-3f_2\right)\sec^2\left(\sqrt{-f_1}\eta\epsilon\right)}\right)^2}{\eta_1^2+\eta_2^2}.$$

Set 18: If $f_1<0$, $f_2>0$, $f_3<0$, $M>0$ and $f_0=0$, then we have the periodic soliton solutions as follows:

$$p_{18}(x,y,t)=e^{i\theta}\left(\frac{12c_2f_1\csc^2\left(\sqrt{-f_1}\eta\epsilon\right)}{2\sqrt{M}-\left(3f_2+\sqrt{M}\right)\csc^2\left(\sqrt{-f_1}\eta\epsilon\right)}+c_0\right),$$

$$q_{18}(x,y,t)=\frac{\delta\eta_1^2\left(\frac{12c_2f_1\csc^2\left(\sqrt{-f_1}\eta\epsilon\right)}{2\sqrt{M}-\left(3f_2+\sqrt{M}\right)\csc^2\left(\sqrt{-f_1}\eta\epsilon\right)}+c_0\right)^2}{\eta_1^2+\eta_2^2}.$$

Set 19: If $f_1<0$, $M>0$ and $f_0=0$, then we have the periodic soliton solutions as follows:

$$p_{19}(x,y,t)=e^{i\theta}\left(\frac{12c_2f_1}{\sqrt{M}\epsilon\cos\left(2\sqrt{-f_1}\eta\right)-3f_2}+c_0\right),$$

$$q_{19}(x,y,t)=\frac{\delta\eta_1^2\left(\frac{12c_2f_1}{\sqrt{M}\epsilon\cos\left(2\sqrt{-f_1}\eta\right)-3f_2}+c_0\right)^2}{\eta_1^2+\eta_2^2}.$$

Set 20: If $f_1<0$, $M>0$ and $f_0=0$, then we have the soliton solutions as follows:

$$p_{20}(x,y,t)=e^{i\theta}\left(\frac{12c_2f_1}{\sqrt{M}\epsilon\sin\left(2\sqrt{-f_1}\eta\right)-3f_2}+c_0\right),$$

$$q_{20}(x,y,t)=\frac{\delta\eta_1^2\left(\frac{12c_2f_1}{\sqrt{M}\epsilon\sin\left(2\sqrt{-f_1}\eta\right)-3f_2}+c_0\right)^2}{\eta_1^2+\eta_2^2}.$$

5. Results and Discussion

In this paper, several soliton solutions for the DSE equation have been described. For this purpose, NMM employed to find some of the new closed-form solitons solutions. While the new mapping method (NMM) itself is not a newly suggested method, the novelty of this research comes from using it for the first time on the fractional (2+1)-dimensional Davey–Stewartson equation with conformable derivatives. The reason behind this selection is that there are many popular analytical techniques that are restricted in the kind

of solutions they can produce. For instance, the tanh-function method is particularly well-suited to generate dark soliton solutions [36], while the Kudryashov method predominantly gives exponential-type solutions [7]. Likewise, the sine–cosine method [37] is limited to periodic wave structures and the Riccati equation method forms rational-type solutions predominantly [17]. The extended trial equation method [18], although efficient, tends to be algebraically cumbersome and does not necessarily provide a wide variety of exact solutions. In contrast, the NMM offers a systematic and adaptable algorithm that allows the derivation of a more extended family of solutions, such as bright, dark, singular, bright–dark, and periodic solitons, all within one framework. This methodological benefit provides more complete analysis of fractional-order effects, especially in tuning soliton amplitude, width, and stability, and thus presents both theoretical richness and practical applicability for nonlinear wave dynamics in fluids, plasmas, and nonlinear optics. In order to place our contribution in context with the wider literature in the area of research in the Davey–Stewartson (DS) system, we present, in Table 1, an overview of some previous studies. This table gives the origin of the DS system, its connection to other governing models, for example, the Benney–Roskes system, as well as major works dealing with integrability, well-posedness, and symmetry analysis. It also critiques popular analytical methods—like trial equation method, extended Weierstrass transformation, simple equation approach, and generalized expansion techniques—which have yielded different categories of solutions in integer-order contexts. In contrast, this current research brings the DS framework to fractional context and uses the new mapping method (NMM) to obtain a significantly larger class of soliton solutions. This gives not just new analytical findings but also new insights into the way fractional parameters affect the soliton dynamics with the prospect of applications in many fields of physics and engineering.

Table 1. Previous studies on the Davey–Stewartson (DS) system and comparison with present work.

Aspect	Previous Studies on DS System	Present Work (Novelty and Applications)
Origin of DS System	Davey and Stewartson [38] derived the DS system in two spatial dimensions using a perturbation expansion to describe the evolution of weakly nonlinear wave packets in finite-depth water.	Builds on this classical DS framework but extends it into the *fractional-order domain* using conformable derivatives.
Relation to Other Models	Shown to be a special case of the Benney–Roskes system [39].	Establishes the DS system's *fractional generalization*, broadening applicability to nonlocal and memory-dependent processes.
Integrability	Integrability studied through the inverse scattering transform (IST) in Ref. [40].	Rather than focusing on integrability, this work applies the *new mapping method (NMM)* to systematically construct exact soliton solutions.
Well-posedness	Investigated in Refs. [41,42] using functional analysis and PDE techniques.	Complements these results by supplying explicit soliton families, illustrating stable/unstable behaviors under fractional effects.

Table 1. *Cont.*

Aspect	Previous Studies on DS System	Present Work (Novelty and Applications)
Symmetry and Algebraic Studies	Champagne & Winternitz studied the Lie symmetry algebra of the DS system.	Goes beyond algebraic structure to provide *constructive analytical soliton solutions* in fractional settings.
Solution Methods	• Gurefe et al.—trial equation method, extended Weierstrass transform [43]. • Zhang et al.—generalized G-expansion for kink/anti-kink solutions [44]. • Stability analysis – simple equation method [45].	Applies the *fractional complex transform with NMM* to generate a *richer family of solutions* (bright, dark, singular, bright–dark, periodic). This provides a unified approach under fractional-order dynamics.
Applications	Mostly focused on mathematical solution construction and theoretical aspects.	Provides *physical interpretation* of fractional parameters (α, β, γ) for controlling soliton amplitude, width, and stability. Potential applications include fluid dynamics, plasma physics, and nonlinear optics (e.g., communication systems, energy transport, photonic device design).

Finally, in this study, by applying Mathematica's symbolic manipulation and consistent methodology, we obtained numerous exact solutions.

The stability of the resultant soliton solutions is presented in Table 2. For all solutions, the table provides the required constraint conditions on the parameters so that the square roots and the denominators are real and well-defined, and thus no imaginary terms are present. All solutions under the given constraints are stable.

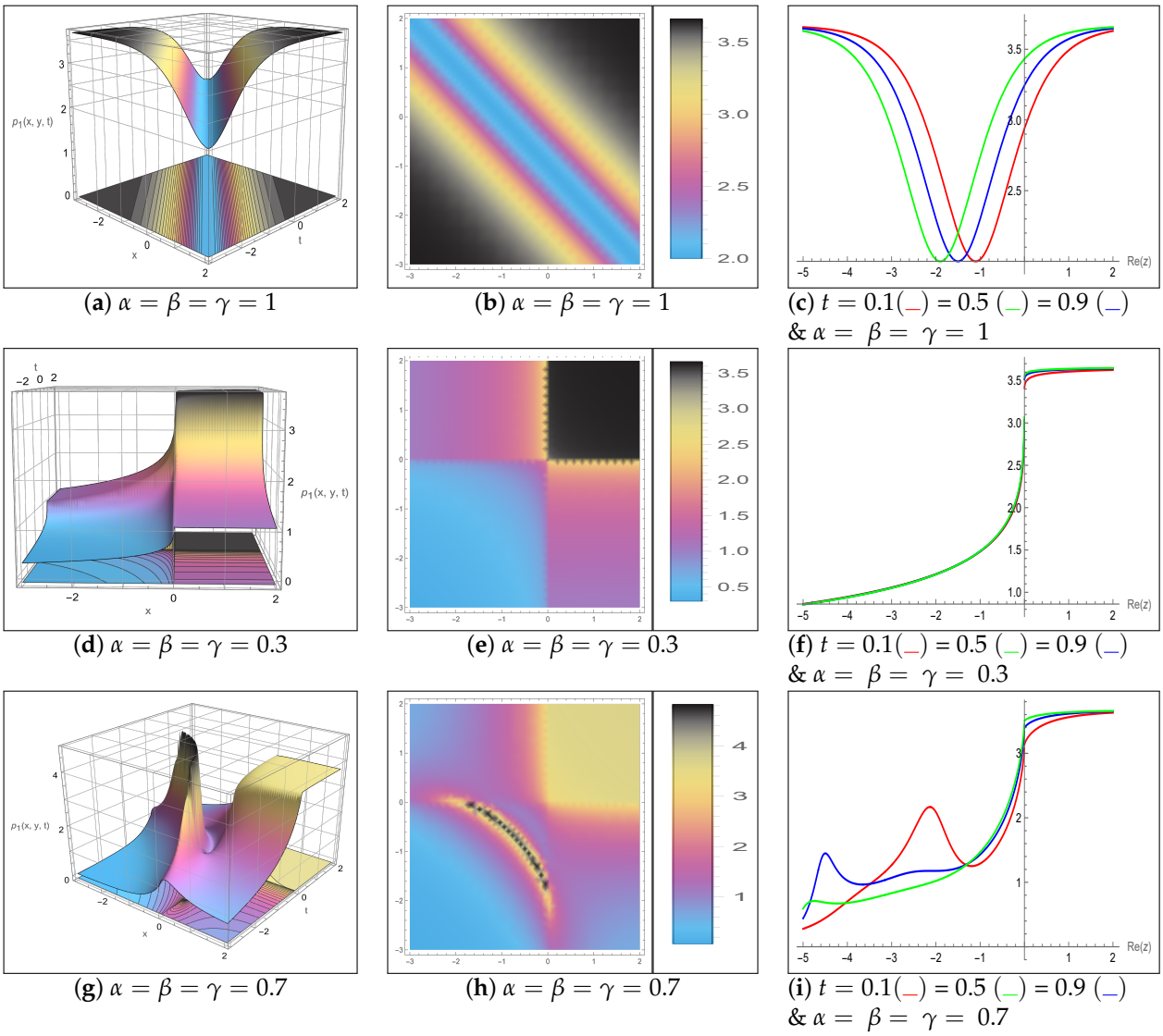
Table 2. Stable solutions with their constraint conditions avoiding imaginary terms.

No.	Solution Name	Constraint Conditions	Stability
1	p_1	$f_1 < 0, f_2 > 0$	Stable
2	p_2	$f_1 < 0, f_2 > 0$	Stable
3	p_3, p_4, p_6, p_{13}, p_{14}	$f_1 > 0$	Stable
4	p_5	$f_1 < 0$	Stable
5	p_7	$f_1 > 0$	Stable
6	p_8	$f_1 < 0, f_3 > 0$	Stable
7	p_9	$f_1 < 0, f_2 < 0$	Stable
8	p_{10}, p_{11}, p_{12}	$f_1 > 0, M > 0$	Stable
9	p_{15}, p_{16}	$f_1 < 0, f_3 > 0$	Stable
10	p_{17}, p_{18}, p_{19}, p_{20}	$f_1 < 0, M > 0$	Stable

Furthermore, by visualizing the functions through 3D contour, density, and 2D plots, such as $|p_1(x,y,t)|$, $|q_1(x,y,t)|$, $|p_2(x,y,t)|$, $|q_2(x,y,t)|$, $|p_9(x,y,t)|$, $|q_9(x,y,t)|$, $|p_{13}(x,y,t)|$, $|q_{13}(x,y,t)|$, $|p_{20}(x,y,t)|$, and $|q_{20}(x,y,t)|$, different solution patterns become visually accessible, revealing various optical soliton solutions.

Figure 1: For visualizing of $|p_1(x,y,t)|$. (a) The 3D contour surface plot shows a dark soliton solution with a distinct peak and symmetric decay over space and time for $\alpha = \beta = \gamma = 1$. (b) A density plot of the same soliton solution representing amplitude variation through color intensity across the xy-plane. (c) A 2D graph illustrating soliton

profiles at different time snapshots, showing the temporal evolution of the soliton shape. (d) The 3D plot illustrates a smooth dark soliton profile with a dip centered in a rising wave structure $\alpha = \beta = \gamma = 0.3$. (e) The density plot reveals a soft color transition with a localized low-amplitude dip, characteristic of dark solitons. (f) The 2D plot shows a gradual dip followed by saturation, indicating a dark soliton behavior in the profile. (g) The 3D plot displays a more pronounced dark soliton with deeper and sharper intensity variations $\alpha = \beta = \gamma = 0.7$. (h) The density plot captures a dark curved path with intensified contrast, suggesting stronger localization. (i) The 2D profile shows oscillatory dips and sharper slopes, reflecting enhanced nonlinearity at higher fractional order for $t = 0.1, 0.5, 0.9$.



(**a**) $\alpha = \beta = \gamma = 1$ (**b**) $\alpha = \beta = \gamma = 1$ (**c**) $t = 0.1$(_) = 0.5 (_) = 0.9 (_) & $\alpha = \beta = \gamma = 1$

(**d**) $\alpha = \beta = \gamma = 0.3$ (**e**) $\alpha = \beta = \gamma = 0.3$ (**f**) $t = 0.1$(_) = 0.5 (_) = 0.9 (_) & $\alpha = \beta = \gamma = 0.3$

(**g**) $\alpha = \beta = \gamma = 0.7$ (**h**) $\alpha = \beta = \gamma = 0.7$ (**i**) $t = 0.1$(_) = 0.5 (_) = 0.9 (_) & $\alpha = \beta = \gamma = 0.7$

Figure 1. Three -dimensional contour plot, density map, and two-dimensional cross-sectional view describing the graphical behavior of dark soliton solution $|p_1(x, y, t)|$ of the fractional $(2+1)$-dimensional Davey–Stewartson equation. Results are displayed for parametric values $\theta_1 = 1$, $\theta_2 = 1, \theta_3 = 1, \eta_1 = 1, \eta_2 = 1, \eta_3 = 1, a = 1, n = 1, b = 1, \lambda = 1, y = 1, c_2 = 1, \epsilon = 1$. The plots illustrate the typical intensity dip of a dark soliton, in which the fractional parameters control the depth, width, and stability of the localized wave structure.

Figure 2: For visualizing of $|q_1(x, y, t)|$. (a) The 3D contour plot for $\alpha = \beta = \gamma = 1$, shows a deep, localized dark soliton dip in the wave profile. (b) A density plot displaying a diagonal dark soliton stripe with symmetric localization in the (x, y) plane. (c) Time evolution showing the propagation of the dark soliton dip. (d) A 3D surface plot showing

a flat-top dark soliton profile with localized dip for $\alpha = \beta = \gamma = 0.3$. (e) A 2D density plot indicating the central dip structure typical of dark solitons. (f) Cross-sectional curves showing a soliton dip with varying real parts, confirming dark soliton behavior. (g) A 3D surface plot with a sharper, localized dip over a broader background stronger dark soliton for $\alpha = \beta = \gamma = 0.7$. (h) A 2D contour/density plot highlighting a more intense dark core region. (i) Line plots showing deepening and broadening soliton dips with increased parameter value, reinforcing dark soliton characteristics for $t = 0.1, 0.5, 0.9$.

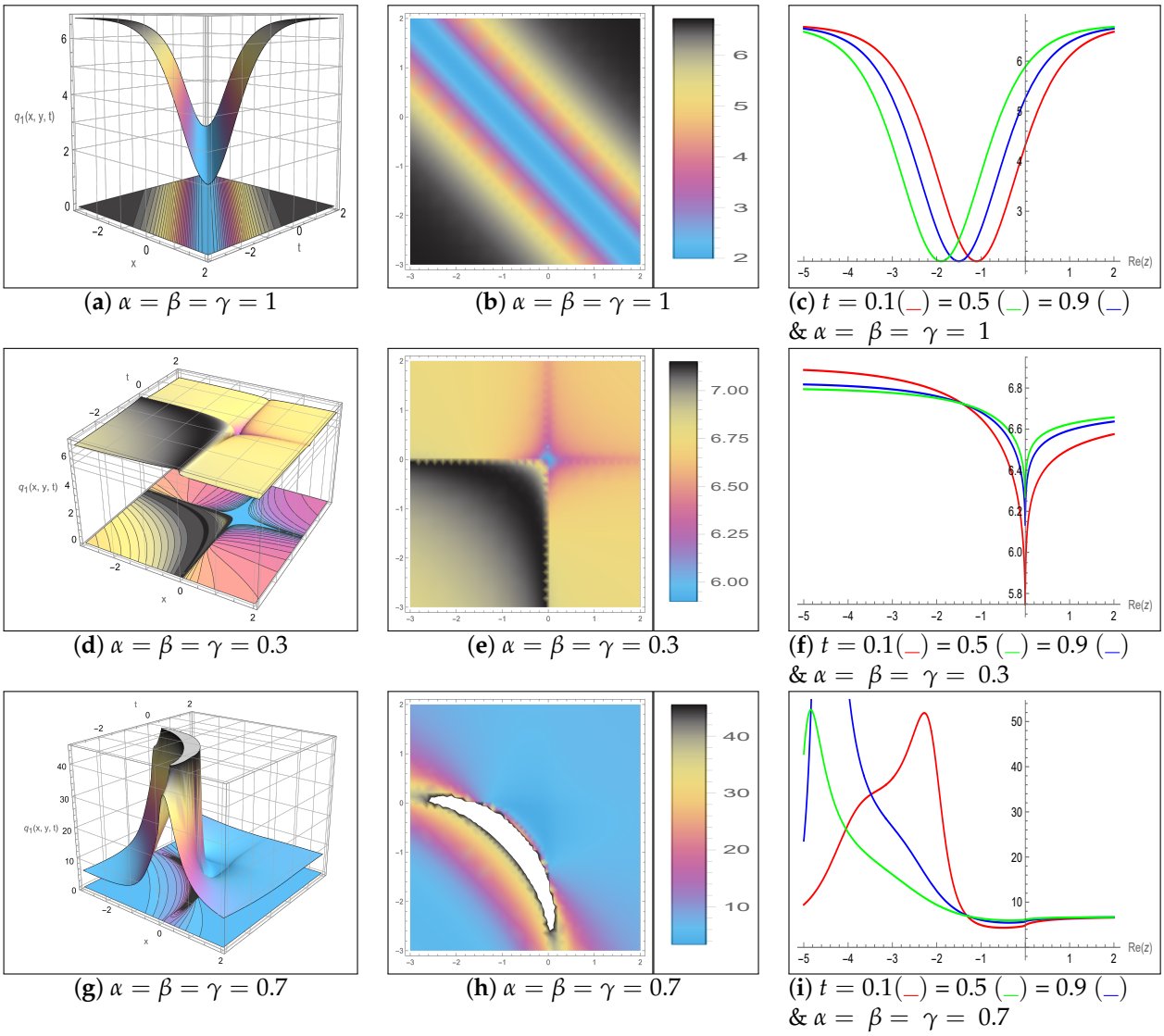
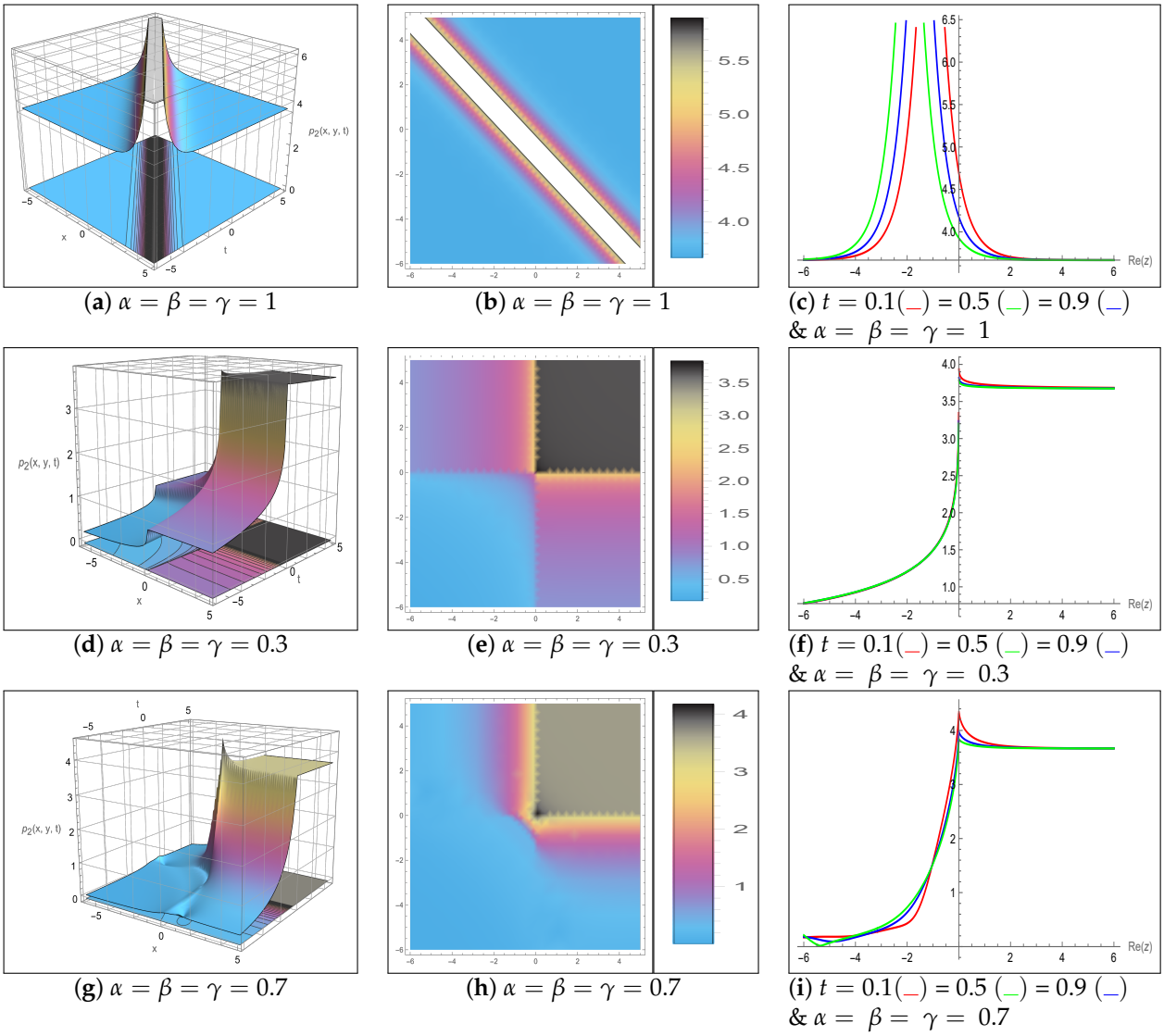


Figure 2. Three-dimensional contour plot, density map, and two-dimensional cross-sectional view exhibiting the graphical behavior of the dark soliton solution $|q_1(x,y,t)|$ of the fractional $(2+1)$-dimensional Davey–Stewartson equation. The simulation is performed for the parametric values $\theta_1 = 1, \theta_2 = 1, \theta_3 = 1, \eta_1 = 1, \eta_2 = 1, \eta_3 = 1, a = 1, n = 1, b = 1, \delta = 1, \lambda = 1, y = 1, c_2 = 1, \epsilon = 1$. The plots evidently show the intensity dip typical of a dark soliton, with fractional parameters affecting the depth, width, and dynamical stability of the soliton.

Figure 3: For visualizing of $|p_2(x,y,t)|$. (a) The 3D contour plot for $\alpha = \beta = \gamma = 1$, shows a a singular soliton solution with a sharp, localized peak along the propagation axis. (b) A corresponding density plot showing a diagonal bright line against a blue background, indicating the localized intensity of the soliton. (c) A 2D line graph displaying the profile of the singular soliton for varying parameters, where the peak sharpness and height vary accordingly. (d) A 3D contour plot displays a sharp singular soliton peak rising steeply

from a smooth background surface for $\alpha = \beta = \gamma = 0.3$. (e) A density plot shows a clear contrast with a distinct singularity region at the center. (f) A 2D plot illustrates the soliton's sharp rise, emphasizing the singular behavior along a specific cross-section. (g) A 3D surface plot demonstrates a more developed soliton with increased height and sharper slope for $\alpha = \beta = \gamma = 0.7$. (h) A density graph highlights a broader and more intense singular region as compared to the lower fractional order. (i) A 2D profile plot reveals higher peaks and steeper gradients, indicating stronger singular behavior at this order for the time $t = 0.1 = 0.5 = 0.9$.



(a) $\alpha = \beta = \gamma = 1$ **(b)** $\alpha = \beta = \gamma = 1$ **(c)** $t = 0.1(_) = 0.5\ (_) = 0.9\ (_)$ & $\alpha = \beta = \gamma = 1$

(d) $\alpha = \beta = \gamma = 0.3$ **(e)** $\alpha = \beta = \gamma = 0.3$ **(f)** $t = 0.1(_) = 0.5\ (_) = 0.9\ (_)$ & $\alpha = \beta = \gamma = 0.3$

(g) $\alpha = \beta = \gamma = 0.7$ **(h)** $\alpha = \beta = \gamma = 0.7$ **(i)** $t = 0.1(_) = 0.5\ (_) = 0.9\ (_)$ & $\alpha = \beta = \gamma = 0.7$

Figure 3. Three-dimensional contour plot, density map, and two-dimensional cross-sectional view describing the graphical behavior of the singular soliton solution $|p_2(x, y, t)|$ of the fractional $(2+1)$-dimensional Davey–Stewartson equation. Plots are produced for parametric values $\theta_1 = 1$, $\theta_2 = 1, \theta_3 = 1, \eta_1 = 1, \eta_2 = 1, \eta_3 = 1, a = 1, n = 1, b = 1, \lambda = 1, y = 1, c_2 = 1, \epsilon = 1$. The graphical solutions show the singular amplitude growth and localized energy accumulation typical of singular solitons, highlighting how fractional parameters affect the emergence and extent of singular behavior.

Figure 4: For visualizing of $|q_2(x, y, t)|$. (a) The 3D contour surface plot shows a sharp singular peak evolving over space and time for $\alpha = \beta = \gamma = 1$. (b) The density plot reveals a white band indicating the unbounded singular region in the spatial–temporal plane. (c) The line graph shows increasing peak sharpness with time, confirming the singular nature of the solution. (d) The 3D contour plot reveals a mild singular soliton structure

with smoother variation and moderate singularity peaks $\alpha = \beta = \gamma = 0.3$. (e) The density plot illustrates a localized bright singularity at the intersection, surrounded by smooth gradients. (f) The 2D plot displays a moderate sharp peak, indicating singular behavior in a narrow region. (g) The 3D contour plot shows a more intense and sharper singular soliton peak with steep rise and deeper valleys $\alpha = \beta = \gamma = 0.7$. (h) The density plot highlights a broader singular zone with increased color intensity, emphasizing nonlinear effects. (i) The 2D plot demonstrates extreme spikes and sharp transitions, confirming stronger singular characteristics at higher fractional orders for $t = 0.1, 0.5, 0.9$.

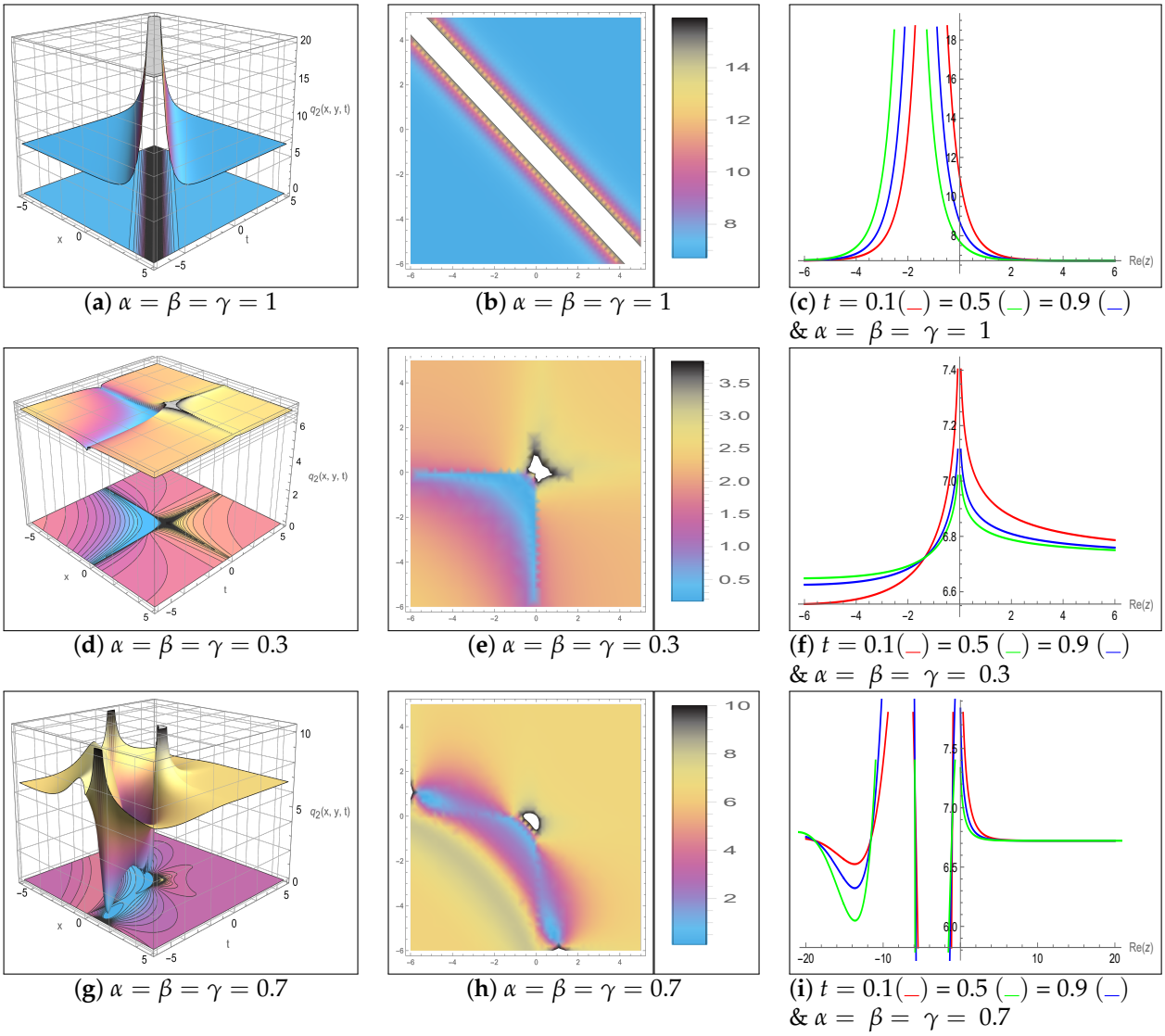


Figure 4. Three-dimensional contour plot, density map, and two-dimensional cross-sectional view describing the graphical behavior of the singular soliton solution $|q_2(x, y, t)|$ of the fractional $(2+1)$-dimensional Davey–Stewartson equation. Plots are produced for parametric values $\theta_1 = 1$, $\theta_2 = 1, \theta_3 = 1, \eta_1 = 1, \eta_2 = 1, \eta_3 = 1, a = 1, n = 1, b = 1, \lambda = 1, y = 1, c_2 = 1, \epsilon = 1$. The graphical solutions show the singular amplitude growth and localized energy accumulation typical of singular solitons, highlighting how fractional parameters affect the emergence and extent of singular behavior.

Figure 5: For visualizing of $|p_9(x, y, t)|$. (a) A 3D contour plot showing a bright soliton peak structure, indicating localization and stability for $\alpha = \beta = \gamma = 1$. (b) A density plot revealing a slightly asymmetric but still bright soliton shape in (x, y) plane. (c) Time evolution of the bright soliton profile for different time steps $t = 0.1, 0.5, 0.9$. (d) A 3D surface plot showing a smooth localized peak, characteristic of a bright soliton for

$\alpha = \beta = \gamma = 0.3$. (e) A 2D density plot indicating a bright spot with a concentrated peak structure. (f) Line plots displaying a soliton profile rising above the background, confirming bright soliton behavior. (g) A 3D plot showing a more intense and sharply rising bright soliton peak for $\alpha = \beta = \gamma = 0.7$. (h) A 2D contour/density plot revealing a strong localized concentration, further supporting bright soliton nature at higher parameter value. (i) Cross-sectional plots illustrating enhanced peak amplitude and steeper gradient for bright solitons as α, β, γ increase.

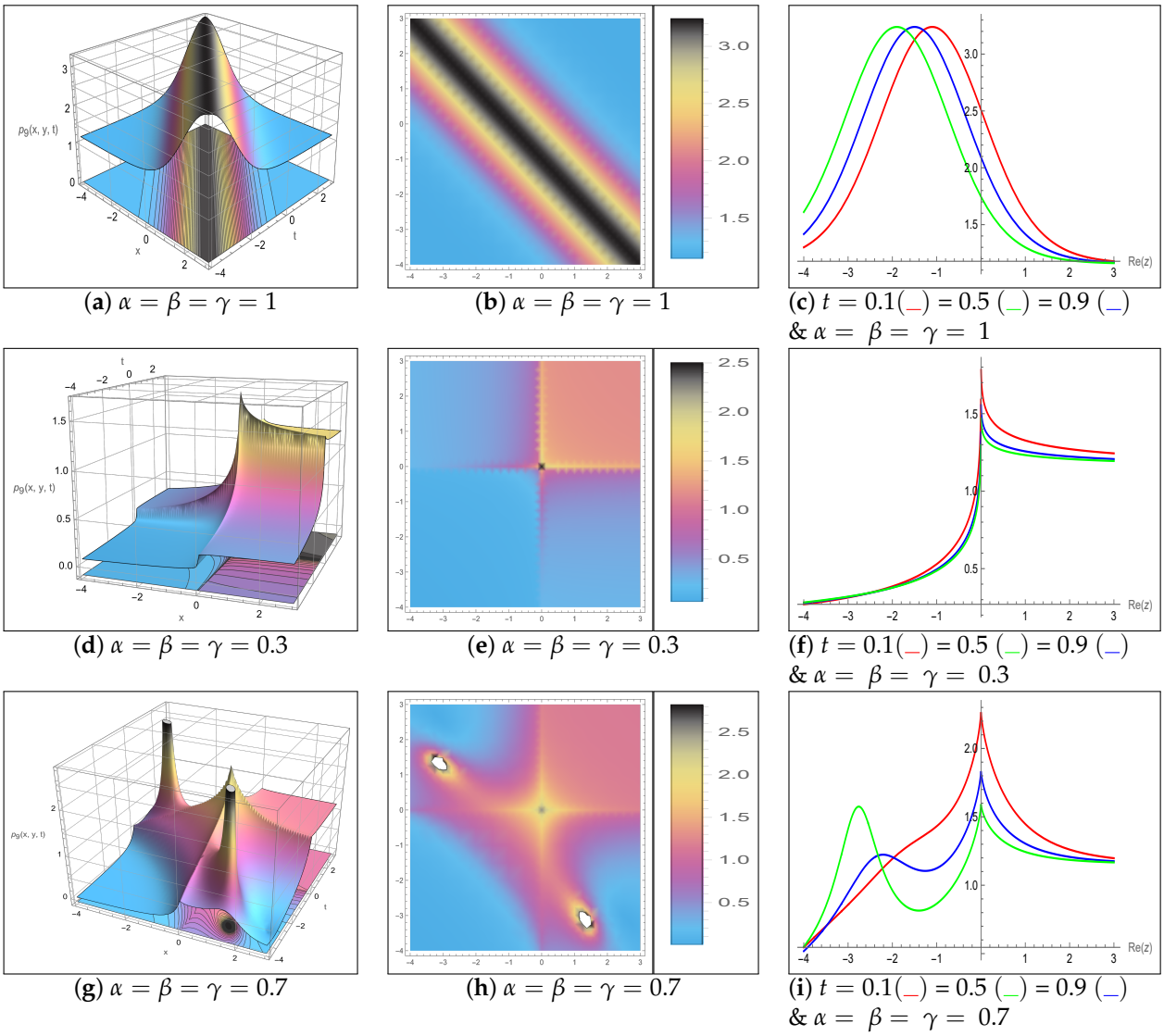


Figure 5. Three-dimensional contour plot, density map, and two-dimensional cross-sectional view illustrating the graphical behavior of the bright soliton solution $|p_9(x, y, t)|$ of the fractional $(2+1)$-dimensional Davey–Stewartson equation. The plots are obtained for parametric values $\theta_1 = 1$, $\theta_2 = 1, \theta_3 = 3, \eta_1 = 1, \eta_2 = 1, \eta_3 = 1, a = -1, n = 1, b = 1, \lambda = 1, y = 1, c_2 = 1, \epsilon = 1, M = 1$. The outcomes obviously show the localized peak structure of a bright soliton, where fractional parameters control the soliton's amplitude, width, and stability, which indicates its controllability in nonlinear fractional media.

Figure 6: For visualizing of $|q_9(x, y, t)|$. (a) A 3D contour plot showing a moderately localized soliton structure for $\alpha = \beta = \gamma = 1$. (b) A density plot revealing a slightly asymmetric but still bright soliton shape in (x, y) plane. (c) Time evolution of the bright soliton profile for different times, showing moderate stability and slight broadening. (d) A 3D surface plot showing a single localized bright peak over a smooth background for

$\alpha = \beta = \gamma = 0.3$. (e) A 2D contour plot illustrating a clear central bright spot confirming the presence of a bright soliton. (f) Line plots showing sharply rising soliton profiles with a bright peak as Re (z) approaches a critical value. (g) A 3D plot showing a taller and sharper bright soliton peak compared to the lower parameter case for $\alpha = \beta = \gamma = 0.7$. (h) A 2D density map highlighting a highly localized bright region, intensified due to higher parameters. (i) Cross-sectional profiles indicating stronger amplitude and narrower width of bright soliton with increasing parameter values for different time steps $t = 0.1, 0.5, 0.9$.

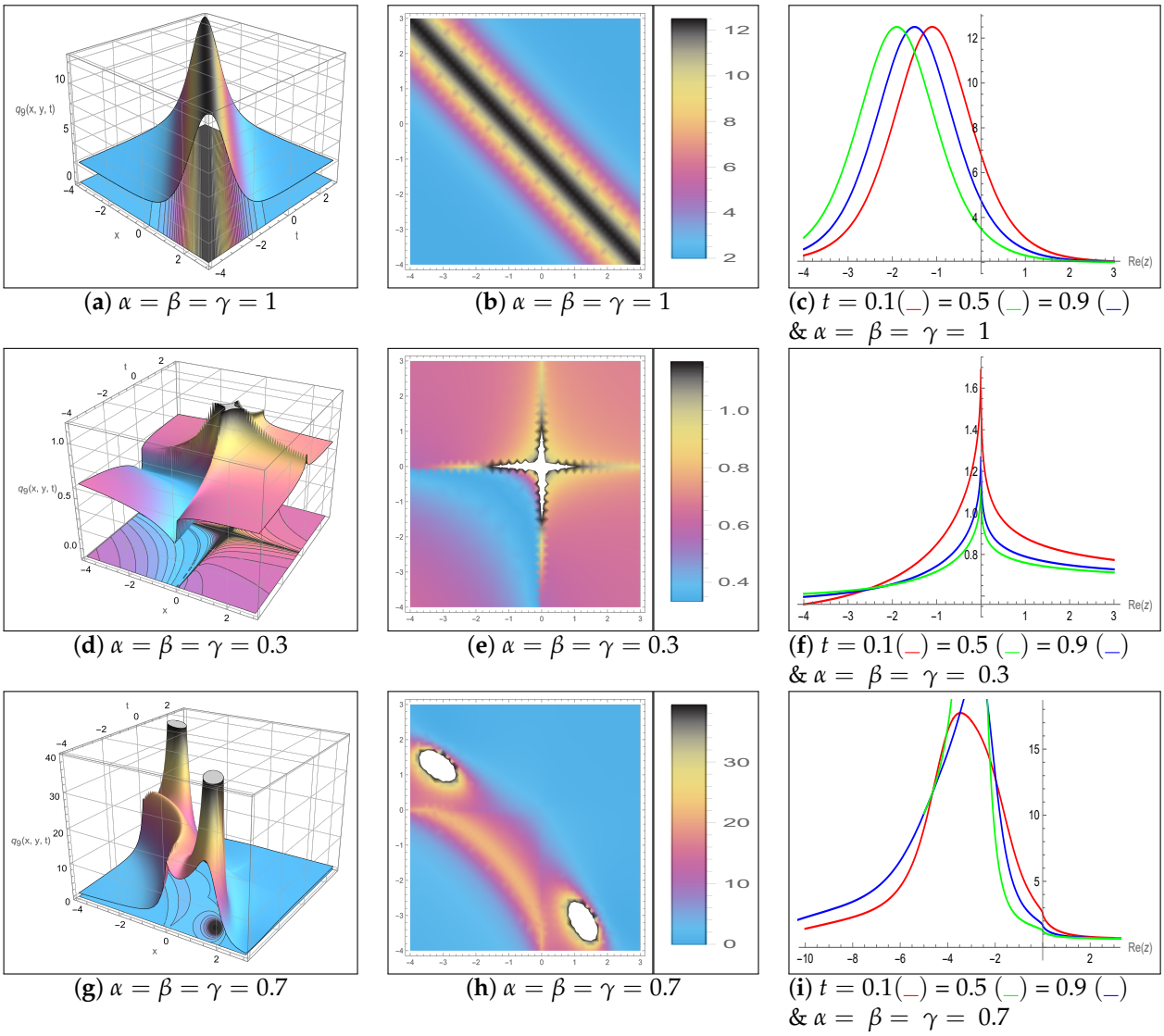


Figure 6. Three-dimensional contour plot, density map, and two-dimensional cross-sectional view illustrating the graphical behavior of the bright soliton solution $|q_9(x, y, t)|$ of the fractional $(2+1)$-dimensional Davey–Stewartson equation. The plots are obtained for parametric values $\theta_1 = 1$, $\theta_2 = 1, \theta_3 = 3, \eta_1 = 1, \eta_2 = 1, \eta_3 = 1, a = -1, n = 1, b = 1, \lambda = 1, y = 1, c_2 = 1, \epsilon = 1, M = 1$. The outcomes obviously show the localized peak structure of a bright soliton, where fractional parameters control the soliton's amplitude, width, and stability, which indicates its controllability in nonlinear fractional media.

Figure 7: For visualizing of $|p_{13}(x, y, t)|$. (a) A 3D contour plot displaying a singular soliton solution with a sharp, steep central spike and abrupt transitions on both sides for $\alpha = \beta = \gamma = 1$. (b) The associated density graph showing a narrow and intense diagonal ridge indicating the position of the singular soliton. (c) A 2D plot showing multiple singular soliton profiles with sharp peaks and rapid drops, reflecting their highly localized and

discontinuous behavior. (d) The 3D surface plot shows a periodic soliton with sharp peaks and oscillatory nature along both spatial and temporal axes for $\alpha = \beta = \gamma = 0.3$. (e) The density plot reveals a concentrated region of high amplitude forming a distinct periodic pattern. (f) The 2D line plot shows periodic waveforms with increasing amplitude, exhibiting singular behavior. (g) The 3D plot illustrates a smoother periodic soliton profile with more pronounced symmetrical structure for $\alpha = \beta = \gamma = 0.7$. (h) The density plot displays a broader and smoother periodic structure compared to lower α, β and γ values. (i) The line plot exhibits multiple peaks and valleys, indicating well-defined periodicity with varied amplitude for different time steps $t = 0.1, 0.5, 0.9$.

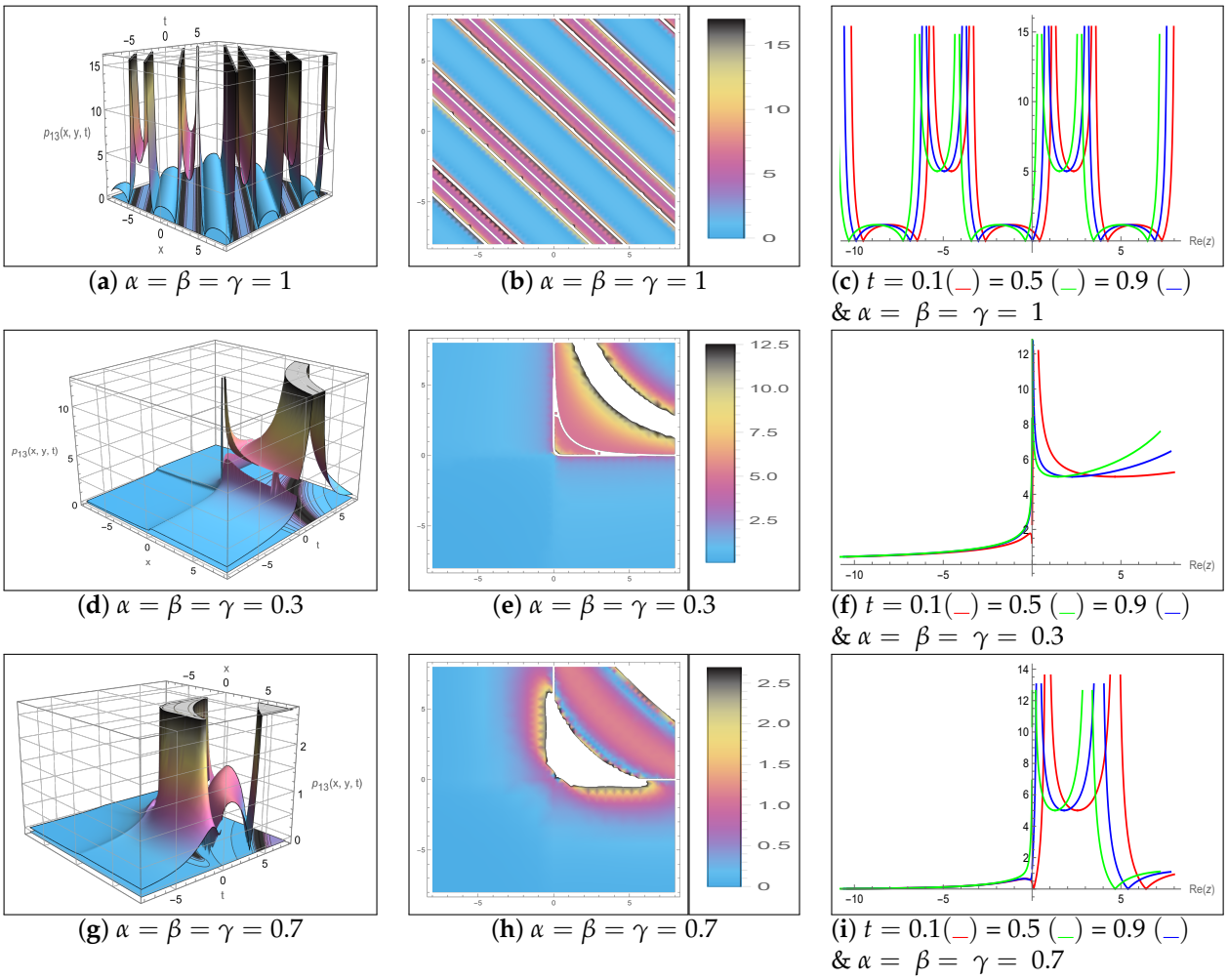


Figure 7. Three-dimensional contour plot, density map, and two-dimensional cross-sectional view demonstrating the graphical behavior of the periodic singular soliton solution $|p_{13}(x, y, t)|$ of the fractional $(2+1)$-dimensional Davey–Stewartson equation. The simulation is performed for parametric values $\theta_1 = 1, \theta_2 = 1, \theta_3 = 3, \eta_1 = 1, \eta_2 = 1, \eta_3 = 1, a = -1, n = 1, b = 1, \lambda = 1, y = 1, c_2 = 1, \epsilon = 1$. The graphical solutions illustrate the coexistence of oscillatory periodic structures and localized singular growth, revealing how fractional parameters control the relationship between regular periodicity and singularity development in nonlinear fractional system.

Figure 8: For visualizing of $|q_{13}(x, y, t)|$. (a) A 3D contour plot displaying a singular soliton solution with a sharp, steep central spike and abrupt transitions on both sides. (b) The associated density graph showing a narrow and intense diagonal ridge indicating the position of the singular soliton. (c) A 2D plot showing multiple singular soliton profiles with sharp peaks and rapid drops, reflecting their highly localized and discontinuous behavior. (d) The 3D plot shows a sharp, localized peak structure with periodic growth in

both spatial and temporal directions for $\alpha = \beta = \gamma = 0.3$. (e) The 2D density plot highlights a high-intensity curved strip indicating a periodic concentration pattern. (f) The 2D line plots display steep, rising oscillations indicating singular-like periodic behavior across different parameters. (g) The 3D surface exhibits a broader, smoother periodic soliton with elevated symmetry and lesser singularity for $\alpha = \beta = \gamma = 0.7$. (h) The density plot reveals periodic wave patterns with smoother transitions and a crescent-shaped high-energy zone. (i) The line graphs show increased periodic oscillations and sharper peaks as α, β and γ values increase.

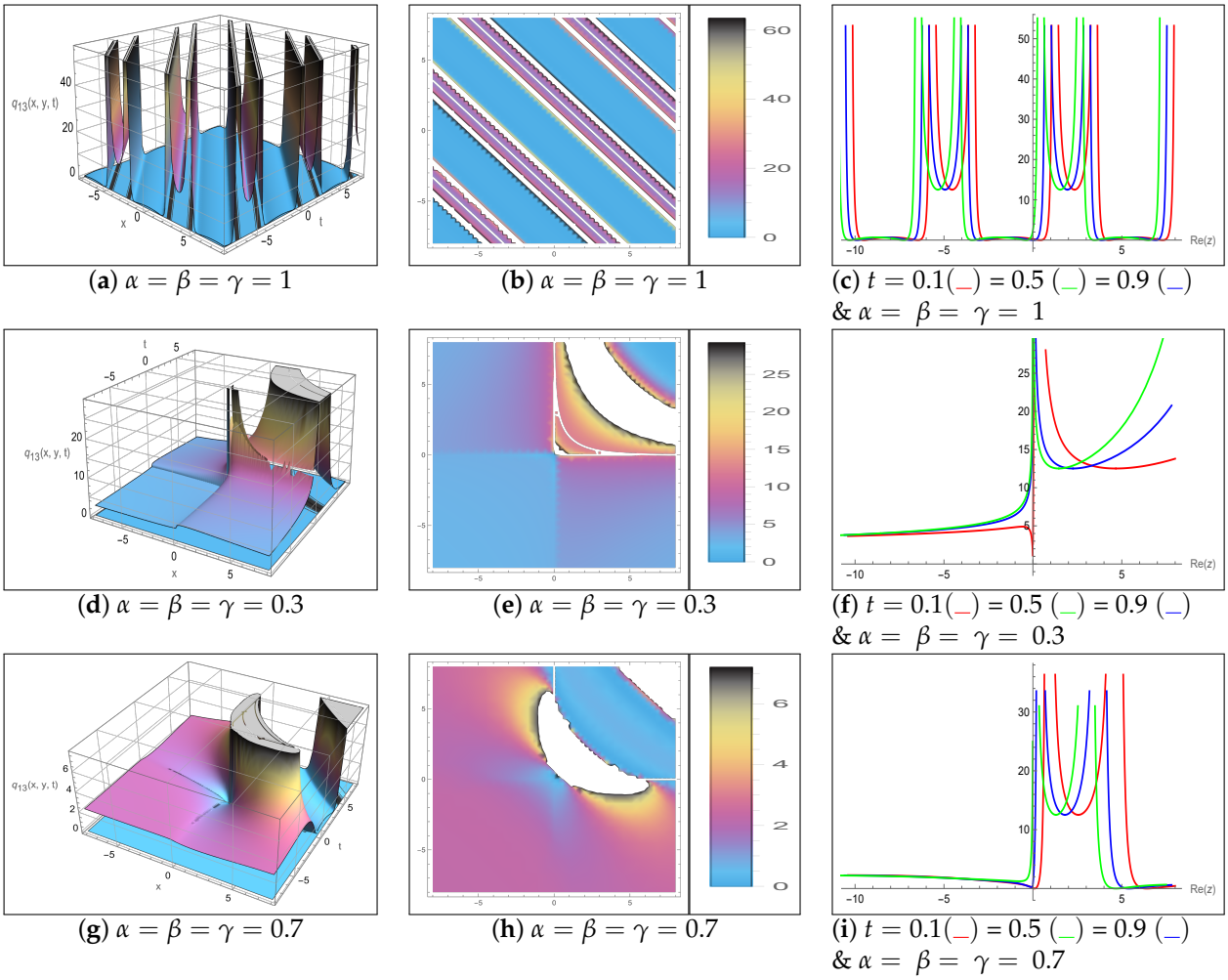


Figure 8. Three-dimensional contour plot, density map, and two-dimensional cross-sectional view demonstrating the graphical behavior of the periodic singular soliton solution $|q_{13}(x, y, t)|$ of the fractional $(2+1)$-dimensional Davey–Stewartson equation. The simulation is performed for parametric values $\theta_1 = 1, \theta_2 = 1, \theta_3 = 3, \eta_1 = 1, \eta_2 = 1, \eta_3 = 1, a = -1, n = 1, b = 1, \lambda = 1, y = 1, c_2 = 1, \epsilon = 1$. The graphical solutions illustrate the coexistence of oscillatory periodic structures and localized singular growth, revealing how fractional parameters control the relationship between regular periodicity and singularity development in nonlinear fractional system.

Figure 9: For visualizing of $|p_{20}(x, y, t)|$. (a) A 3D contour plot displaying sharply localized, high-amplitude peaks, indicating a periodic, singular soliton structure for $\alpha = \beta = \gamma = 1$. (b) The density plot reveals a diagonal arrangement of intense, localized structures with irregular spacing, suggesting periodic or singular soliton behavior. (c) The 2D line plot presents steep, isolated spikes with asymmetric profiles, consistent with periodic, singular soliton solutions at different time snapshots for different time steps $t = 0.1, 0.5, 0.9$. (d) The 3D plot illustrates a localized periodic soliton peak with rapid

elevation and smooth decay for $\alpha = \beta = \gamma = 0.3$. (e) The 2D contour plot highlights two symmetric high-intensity zones representing periodic energy concentrations. (f) The 2D graph shows distinct wave profiles with oscillatory growth and inflection points along the x-axis. (g) The 3D surface reveals a broader and more defined periodic structure with a shifted central peak for $\alpha = \beta = \gamma = 0.7$. (h) The 2D density plot displays a crescent-shaped high-energy path, indicating periodic propagation with sharp gradients. (i) The line plot shows enhanced periodic oscillations with varied peak locations across different wave modes.

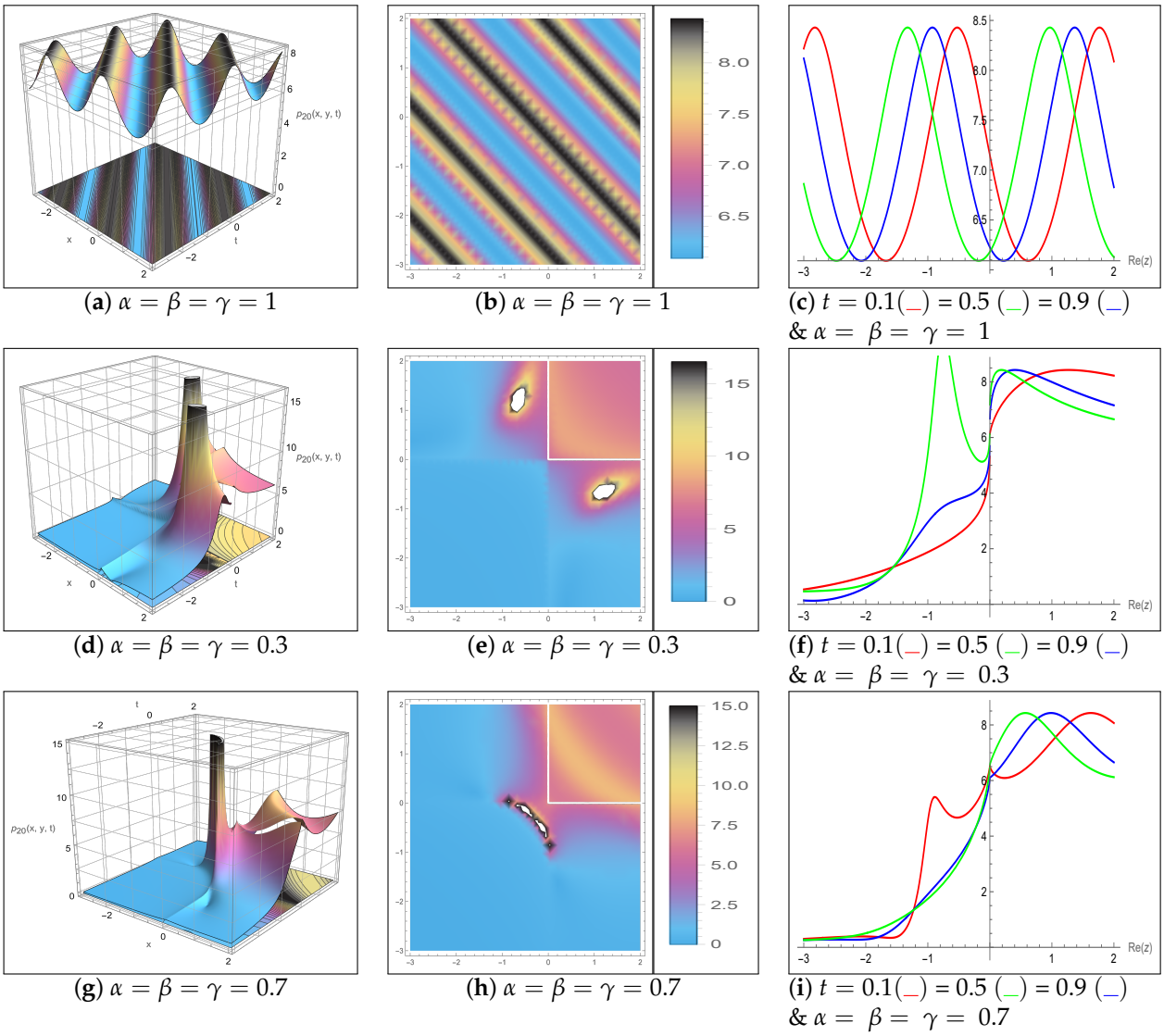


Figure 9. Three-dimensional contour plot, density map, and two-dimensional cross-sectional view showing the graphical behavior of the periodic soliton solution $|p_{20}(x, y, t)|$ of the fractional $(2+1)$-dimensional Davey–Stewartson equation. The plots correspond to parametric values $\theta_1 = 1$, $\theta_2 = 1, \theta_3 = 1, \eta_1 = 1, \eta_2 = 1, \eta_3 = 1, a = 1, n = 1, b = 1, \lambda = 1, y = 1, c_2 = 1, \epsilon = 1$. The graphical results highlight the oscillatory wave structure characteristic of periodic solitons, with fractional parameters modulating amplitude, wavelength, and stability of the periodic pattern.

Figure 10: For visualizing of $|q_{20}(x, y, t)|$. (a) A 3D contour surface plot shows sharply localized, high-amplitude peaks, indicating a periodic, singular soliton structure. (b) The density plot reveals a diagonal arrangement of intense, localized structures with irregular spacing, suggesting periodic or singular soliton behavior. (c) The 2D line plot presents steep, isolated spikes with asymmetric profiles, consistent with non-periodic, singular soliton solutions at different time snapshots. (d) The 3D plot shows periodic soliton peaks

forming localized structures along the x-t plane for $\alpha = \beta = \gamma = 0.3$. (e) The 2D density plot reveals symmetric bright soliton structures with periodic spatial pattern. (f) Line graph displays periodic amplitude oscillations of solitons for different time slices. (g) The 3D surface depicts more pronounced and wider periodic soliton pulses than at lower parameter values for $\alpha = \beta = \gamma = 0.7$. (h) The density plot highlights broader and merged periodic soliton structures indicating increased interaction. (i) The curves show stronger and more separated peaks in soliton amplitude with increasing α, β and γ.

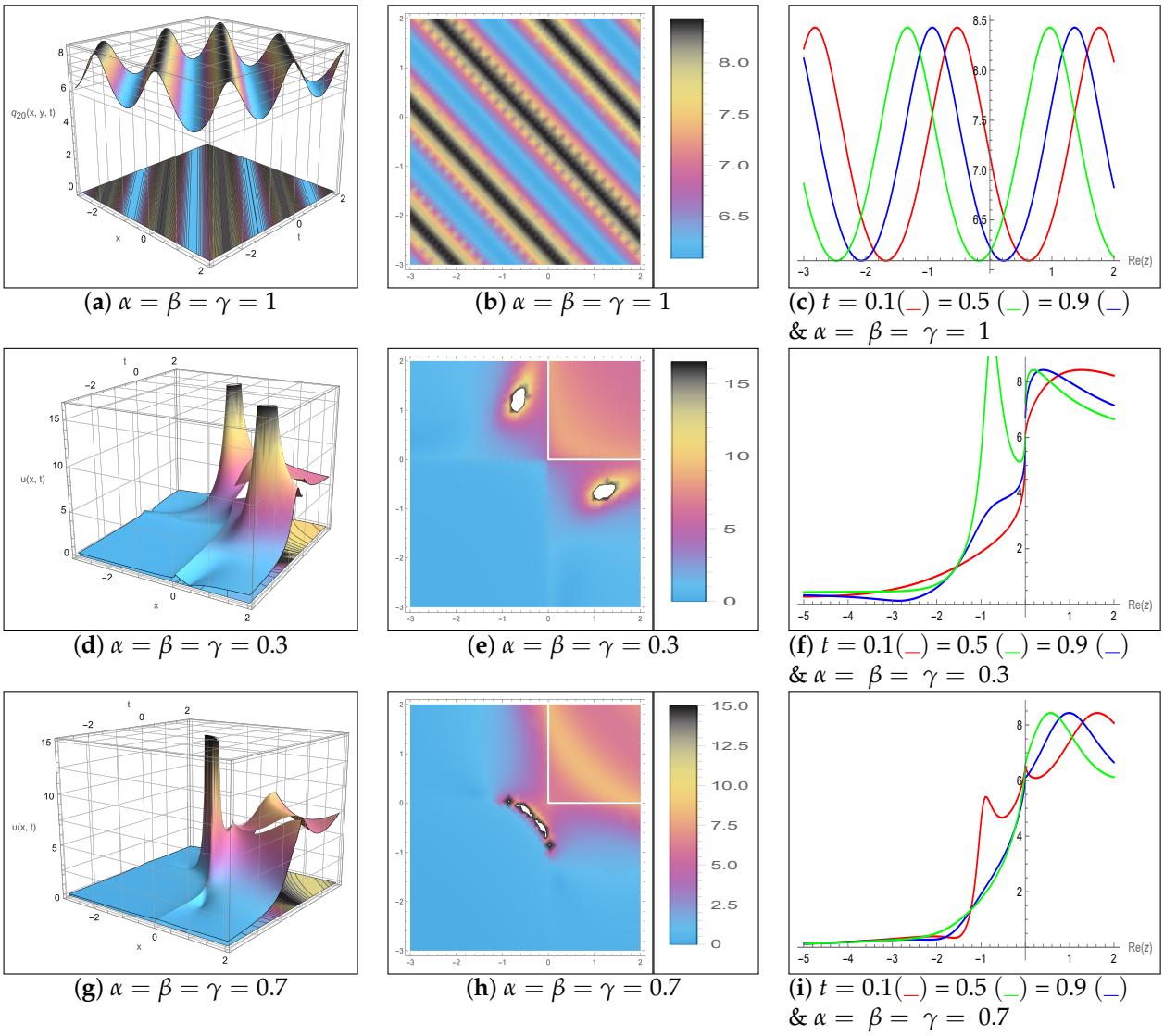


Figure 10. Three-dimensional contour plot, density map, and two-dimensional cross-sectional view showing the graphical behavior of the periodic soliton solution $|q_{20}(x, y, t)|$ of the fractional $(2+1)$-dimensional Davey–Stewartson equation. The plots correspond to parametric values $\theta_1 = 1$, $\theta_2 = 1, \theta_3 = 1, \eta_1 = 1, \eta_2 = 1, \eta_3 = 1, a = 1, n = 1, b = 1, \lambda = 1, y = 1, c_2 = 1, \epsilon = 1$. The graphical results highlight the oscillatory wave structure characteristic of periodic solitons, with fractional parameters modulating amplitude, wavelength, and stability of the periodic pattern.

6. Conclusions

The current study contributes significantly to developing the theoretical and applied knowledge on nonlinear wave propagation in fractional systems. Using a fractional-order formulation, the research proves that fractional derivatives better describe anomalous dispersion, memory effects, and fractal geometries compared to traditional integer-order methods, thus yielding a more robust and realistic description of physical processes.

The main goal of this paper was to build and study soliton solutions of the fractional (2+1)-dimensional Davey–Stewartson equation and observe in detail the impact of varying fractional orders on soliton amplitude, width, and stability. To this end, the Davey–Stewartson system was reduced to a system of nonlinear ordinary differential equations by using the fractional complex transform. The equations were subsequently solved with a new mapping technique that allowed the derivation of a wide family of exact soliton solutions such as bright, dark, singular, bright–dark, and periodic structures.

The method used in this work was both powerful and adaptable. The fractional complex transform, which was developed from local fractional calculus on the fractal domain, was a good bridge between fractional differential equations and solvable nonlinear ODEs. By using this systematic process, various classes of soliton solutions were successfully built and their characteristics under the action of fractional parameters α, β, and γ were explored in detail. Graphical computations by way of contour maps, density plots, and cross-profiles validated the stability of the derived solutions and reaffirmed the pronounced impact of fractional-order effects on nonlinear wave propagation.

The main conclusion reached from this work is that the joint use of the fractional complex transform and the new mapping technique provides an effective analytical model for synthesizing various families of solitons in fractional systems. The research verifies that fractional parameters give a tunable mechanism for the manipulation of soliton dynamics, and thus new avenues for designing and optimizing applied systems in plasma physics, fluid dynamics, and nonlinear optics. Additionally, by contrasting fractional-order solutions with integer-order versions of them, the research emphasizes the efficacy of fractional calculus in simulating realistic, nonlocal, and memory-dependent physical systems. In general, this work not only extends soliton theory to the realm of fractional calculus but also sets the groundwork for subsequent endeavors in nonlinear fractional systems. The newly found exact solitary wave solutions presented here—not previously explored in existing research—are a point of departure for further studies in fractional models from physics to applied mathematics to next-generation technological applications.

In future research, the stochastic fractional Davey–Stewartson equation could be investigated to capture random perturbations with noise influence in actual physical systems and activation of shock waves [46]. The current analysis is performed within the context of the conformable (local) fractional derivative with the fractional parameters confined to $\alpha, \beta, \gamma \in (0, 1]$. Additionally, the resulting soliton solutions are only valid under the constraint conditions of the given proposed method, and hence the methodological constraint of the present research study lies here.

Author Contributions: Conceptualization, E.M.A.-D.; methodology, M.T.; software, M.T.; formal analysis, E.K.J.; investigation, E.K.J.; writing—original draft preparation, M.T.; writing—review and editing, E.K.J. and E.M.A.-D.; supervision, H.U.R.; project administration, E.M.A.-D.; funding acquisition, E.K.J. All authors have read and agreed to the published version of the manuscript.

Funding: This work was supported and funded by the Deanship of Scientific Research at Imam Mohammad Ibn Saud Islamic University (IMSIU) (grant number IMSIU-DDRSP2502).

Data Availability Statement: All the data used during this study are accessible within the manuscript.

Conflicts of Interest: The authors declare no conflicts of interest.

References

1. Bullough, R.K.; Caudrey, P.J. The soliton and its history. In *Solitons*; Springer: Berlin/Heidelberg, Germany, 1980; pp. 1–64.
2. Chen, Z.; Segev, M.; Christodoulides, D.N. Optical spatial solitons: Historical overview and recent advances. *Rep. Prog. Phys.* **2012**, *75*, 086401. [CrossRef] [PubMed]

3. Hasegawa, A. An historical review of application of optical solitons for high speed communications. *Chaos Interdiscip. J. Nonlinear Sci.* **2000**, *10*, 475–485. [CrossRef]
4. Stegeman, G.I.; Christodoulides, D.N.; Segev, M. Optical spatial solitons: Historical perspectives. *IEEE J. Sel. Top. Quantum Electron.* **2002**, *6*, 1419–1427. [CrossRef]
5. Rehman, H.U.; Tehseen, M.; Ashraf, H.; Awan, A.U.; Ali, M.R. Unveiling dynamic solitons in the (2+1)-dimensional Kadomtsev–Petviashvili equation: Insights from fluids and plasma. *Partial. Differ. Equ. Appl. Math.* **2004**, *9*, 100633. [CrossRef]
6. Bai, C.L.; Zhao, H. Complex-Hyperbolic-Funct. Method Its Appl. Nonlinear Equations. *Phys. Lett. A* **2006**, *355*, 32–38. [CrossRef]
7. Kudryashov, N.A. Method for finding optical solitons of generalized nonlinear Schrödinger equations. *Optik* **2022**, *261*, 169163. [CrossRef]
8. Yang, X.F.; Deng, Z.C.; Wei, Y. A Riccati–Bernoulli sub-ODE method for nonlinear partial differential equations and its application. *Adv. Differ. Equ.* **2015**, *2015*, 117. [CrossRef]
9. Yang, Z.; Hon, B.Y. An improved modified extended tanh-function method. *Z. Naturforschung A* **2006**, *61*, 103–115. [CrossRef]
10. Ozdemir, N. Optical solitons for the Biswas–Milovic equation with anti-cubic law nonlinearity in the presence of spatio-temporal dispersion. *Phys. Scr.* **2023**, *98*, 085229. [CrossRef]
11. Aljahdaly, N.H. Some applications of the modified (G'/G^2)-expansion method in mathematical physics. *Results Phys.* **2019**, *13*, 102272. [CrossRef]
12. Manafian, J.; Lakestani, M. Application of tan $(\Phi/2)$-expansion method for solving the Biswas–Milovic equation for Kerr law nonlinearity. *Optik* **2016**, *127*, 2040–2054. [CrossRef]
13. Vitanov, N.K. On modified method of simplest equation for obtaining exact and approximate solutions of nonlinear PDEs: The role of the simplest equation. *Commun. Nonlinear Sci. Numer. Simul.* **2011**, *16*, 4215–4231. [CrossRef]
14. He, J.H. Variational iteration method–a kind of non-linear analytical technique: Some examples. *Int. J. Non-Linear Mech.* **1999**, *34*, 699–708. [CrossRef]
15. Akcagil, S.; Aydemir, T. A new application of the unified method. *New Trends Math. Sci.* **2018**, *6*, 185–199. [CrossRef]
16. Kudryashov, N.A.; Soukharev, M.B. Popular Ansatz methods and Solitary wave solutions of the Kuramoto-Sivashinsky equation. *Regul. Chaotic Dyn.* **2009**, *14*, 407–419. [CrossRef]
17. Bittanti, S.; Colaneri, P.; De Nicolao, G. The periodic Riccati equation. In *The Riccati Equation*; Springer: Berlin/Heidelberg, Germany, 1991; pp. 127–162.
18. Rezazadeh, H.; Korkmaz, A.; Eslami, M.; Mirhosseini-Alizamini, S.M. A large family of optical solutions to Kundu–Eckhaus model by a new auxiliary equation method. *Opt. Quantum Electron.* **2019**, *51*, 84. [CrossRef]
19. Hosseini, K.; Mirzazadeh, M.; Ilie, M.; Gómez-Aguilar, J.F. Biswas–Arshed equation with the beta time derivative: Optical solitons and other solutions. *Optik* **2020**, *217*, 164801. [CrossRef]
20. Ullah, N.; Rehman, H.U.; Asjad, M.I.; Riaz, M.B.; Muhammad, T. Wave analysis in generalized fractional Tzitzéica-type nonlinear PDEs: Contributions to nonlinear sciences. *Alex. Eng. J.* **2024**, *92*, 102–116. [CrossRef]
21. Zulfiqar, H.; Aashiq, A.; Tariq, K.U.; Ahmad, H.; Almohsen, B.; Aslam, M.; Rehman, H.U. On the solitonic wave structures and stability analysis of the stochastic nonlinear Schrödinger equation with the impact of multiplicative noise. *Optik* **2023**, *289*, 171250. [CrossRef]
22. Rehman, H.U.; Ullah, N.; Imran, M.A.; Akgül, A. Optical solitons of two non-linear models in birefringent fibres using extended direct algebraic method. *Int. J. Appl. Comput. Math.* **2021**, *7*, 227. [CrossRef]
23. Cevikel, A.C.; Aksoy, E. Soliton solutions of nonlinear fractional differential equations with their applications in mathematical physics. *Rev. Mex. Física* **2021**, *67*, 422–428. [CrossRef]
24. Guner, O.; Bekir, A. Bright and dark soliton solutions for some nonlinear fractional differential equations. *Chin. Phys. B* **2016**, *25*, 030203. [CrossRef]
25. Özkan, E.M.; Özkan, A. The soliton solutions for some nonlinear fractional differential equations with Beta-derivative. *Axioms* **2021**, *10*, 203. [CrossRef]
26. Akram, G.; Arshed, S.; Sadaf, M. Soliton solutions of generalized time-fractional Boussinesq-like equation via three techniques. *Chaos Solitons Fractals* **2023**, *173*, 113653. [CrossRef]
27. Akram, G.; Sadaf, M.; Mariyam, H. A comparative study of the optical solitons for the fractional complex Ginzburg–Landau equation using different fractional differential operators. *Optik* **2022**, *256*, 168626. [CrossRef]
28. Wang, B.H.; Wang, Y.Y.; Dai, C.Q.; Chen, Y.X. Dynamical characteristic of analytical fractional solitons for the space-time fractional Fokas-Lenells equation. *Alex. Eng. J.* **2020**, *59*, 4699–4707. [CrossRef]
29. Malomed, B.A. Optical solitons and vortices in fractional media: A mini-review of recent results. *Photonics* **2021**, *8*, 353. [CrossRef]
30. Ullah, N.; Asjad, M.I.; Awrejcewicz, J.; Muhammad, T.; Baleanu, D. On soliton solutions of fractional-order nonlinear model appears in physical sciences. *AIMS Math.* **2022**, *7*, 7421–7440. [CrossRef]
31. Ahmad, J.; Mustafa, Z. Analysis of soliton solutions with different wave configurations to the fractional coupled nonlinear Schrödinger equations and applications. *Opt. Quantum Electron.* **2023**, *55*, 1228. [CrossRef]

32. Saha Ray, S. New exact solutions of fractional Davey-Stewartson equation with power-law nonlinearity and new integrable Davey-Stewartson-type equation. *Eur. Phys. J. Plus* **2016**, *131*, 1–11. [CrossRef]
33. Alngar, M.E.; Alamri, A.M.; AlQahtani, S.A.; Shohib, R.M.; Pathak, P. Exploring optical soliton solutions in highly dispersive couplers with parabolic law nonlinear refractive index using the extended auxiliary equation method. *Mod. Phys. Lett. B* **2024**, *38*, 2450350. [CrossRef]
34. Rehman, H.U.; Awan, A.U.; Tag-ElDin, E.M.; Alhazmi, S.E.; Yassen, M.F.; Haider, R. Extended hyperbolic function method for the (2+1)-dimensional nonlinear soliton equation. *Results Phys.* **2022**, *40*, 105802. [CrossRef]
35. Zayed, E.M.; Alurrfi, K.A.; Alshbear, R.A. On application of the new mapping method to magneto-optic waveguides having Kudryashov's law of refractive index. *Optik* **2023**, *287*, 171072. [CrossRef]
36. Wazwaz, A.M. The tanh method and the sine–cosine method for solving the KP-MEW equation. *Int. J. Comput. Math.* **2005**, *82*, 235–246. [CrossRef]
37. Wazwaz, A.M. A sine-cosine method for handling nonlinear wave equations. *Math. Comput. Modelling* **2004**, *40*, 499–508. [CrossRef]
38. Davey, A.; Stewartson, K. On three-dimensional packets of surface waves. *Proc. R. Soc. London Ser. A* **1974**, *338*, 101–110.
39. Benney, D.J.; Roskes, G.J. Wave instabilities. *Stud. Appl. Math.* **1969**, *48*, 377–385. [CrossRef]
40. Fokas, A.S. Inverse scattering of first-order systems in the plane related to nonlinear multidimensional equations. *Phys. Rev. Lett.* **1983**, *51*, 3. [CrossRef]
41. Ghidaglia , J.M.; Saut, J.C. On the initial value problem for the Davey--Stewartson systems. *Nonlinearity* **1990**, *3*, 475. [CrossRef]
42. Sugimoto, M.; Wang, B.; Zhang, R. Local well-posedness for the Davey–Stewartson equation in a generalized Feichtinger algebra. *J. Fourier Anal. Appl.* **2015**, 21, 1105–1129. [CrossRef]
43. Gurefe, Y.; Misirli, E.; Pandir, Y.; Abdullah, S.; Mehmet, E. New exact solutions of the Davey–Stewartson equation with power-law nonlinearity. *Bull. Malays. Math. Sci. Soc.* **2015**, *38*, 1223–1234. [CrossRef]
44. Zhang, B.; Xiong, M.; Chen, L. Many new exact solutions for generalized Davey-Stewartson equation with arbitrary power nonlinearities using novel. *J. Adv. Appl. Math.* **2019**, *4*, 11. [CrossRef]
45. Selima, E.S.; Seadawy, A.R.; Yao, X. The nonlinear dispersive Davey--Stewartson system for surface waves propagation in shallow water and its stability. *Eur. Phys. J. Plus* **2016**, *131*, 425. [CrossRef]
46. Wang, Z.; Yao, K.; Chang, J.; Yue, L.; Chen, H.; Huang, R.; Chao, Y. Experimental investigation of shock-wave–streamwise-vortex interaction. *AIAA J.* **2025**, *63*, 3079–3106. [CrossRef]

Disclaimer/Publisher's Note: The statements, opinions and data contained in all publications are solely those of the individual author(s) and contributor(s) and not of MDPI and/or the editor(s). MDPI and/or the editor(s) disclaim responsibility for any injury to people or property resulting from any ideas, methods, instructions or products referred to in the content.